Journal of Medicinal Chemistry

Article

Cite This: J. Med. Chem. 2019, 62, 512−530

pubs.acs.org/jmc

New Water-Soluble Copper(II) Complexes with Morpholine−Thiosemicarbazone Hybrids: Insights into the Anticancer and Antibacterial Mode of Action

Kateryna Ohui,[†,††] Eleonora Afanasenko,[†,††] Felix Bacher,[†] Rachel Lim Xue Ting,[‡] Ayesha Zafar,[§] Núria Blanco-Cabra,[∥] Eduard Torrents,[∥] Orsolya Dömötör,[⊥] Nóra V. May,[#] Denisa Darvasiova,[¶] Éva A. Enyedy,[⊥] Ana Popović-Bijelić,[▽] Jóhannes Reynisson,[§] Peter Rapta,[¶] Maria V. Babak,*[,○,◆] Giorgia Pastorin,[‡] and Vladimir B. Arion*[,†]

[†]Institute of Inorganic Chemistry, University of Vienna, Währinger Strasse 42, A-1090 Vienna, Austria

[‡]Department of Pharmacy, National University of Singapore, 3 Science Drive 2, Singapore 117543, Singapore

[§]School of Chemical Sciences, University of Auckland, Auckland 1010, New Zealand

[∥]Bacterial Infections: Antimicrobial Therapies, Institute for Bioengineering of Catalonia (IBEC), The Barcelona Institute of Science and Technology, Barcelona 08036, Spain

[⊥]Department of Inorganic and Analytical Chemistry, University of Szeged, Dóm tér 7., H-6720 Szeged, Hungary

[#]Research Centre of Natural Sciences, Hungarian Academy of Sciences, Magyar tudósok körútja 2., H-1117 Budapest, Hungary

[¶]Institute of Physical Chemistry and Chemical Physics, Slovak Technical University of Technology, Radlinského 9, 81237 Bratislava, Slovak Republic

[▽]Faculty of Physical Chemistry, University of Belgrade, 11158 Belgrade, Serbia

[○]Department of Chemistry, National University of Singapore, 3 Science Drive 2, 117543, Singapore

[◆]Drug Development Unit, National University of Singapore, 28 Medical Drive, 117546, Singapore

Supporting Information

ABSTRACT: Six morpholine-(iso)thiosemicarbazone hybrids HL^1−HL^6 and their Cu(II) complexes with good-to-moderate solubility and stability in water were synthesized and characterized. Cu(II) complexes $[Cu(L^{1-6})Cl]$ (**1**−**6**) formed weak dimeric associates in the solid state, which did not remain intact in solution as evidenced by ESI-MS. The lead proligands and Cu(II) complexes displayed higher antiproliferative activity in cancer cells than triapine. In addition, complexes **2**−**5** were found to specifically inhibit the growth of Gram-positive bacteria *Staphylococcus aureus* with MIC_{50} values at 2−5 μg/mL. Insights into the processes controlling intracellular accumulation and mechanism of action were investigated for **2** and **5**, including the role of ribonucleotide reductase (RNR) inhibition, endoplasmic reticulum stress induction, and regulation of other cancer signaling pathways. Their ability to moderately inhibit R2 RNR protein in the presence of dithiothreitol is likely related to Fe chelating properties of the proligands liberated upon reduction.

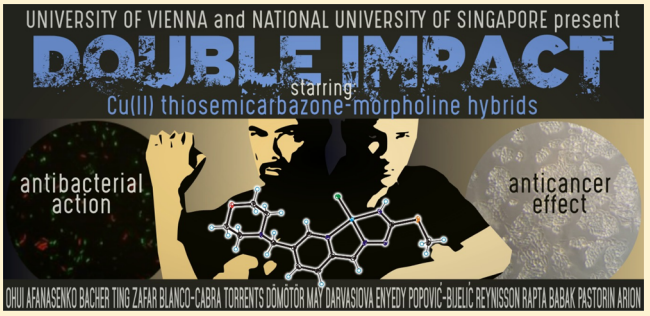

1. INTRODUCTION

Progress in modern anticancer therapy has led to significant improvements in survival rates of cancer patients. However, even though more patients achieve remission nowadays, their lifespan often remains short.[1] One of the major causes of cancer death is the malignant process itself, which is associated with extensive formation of metastases, but it is not commonly mentioned that a significant number of immunocompromised cancer patients die due to infections, such as pneumonia and peritonitis.[2] Despite that cancer patients are very prone to develop infections during chemotherapy, their preventive antibiotic treatment is hampered by additional adverse effects.[3] However, recent clinical evidence demonstrated that benefits of antibiotic prophylaxis of cancer patients outweighed its risks.[4] The simultaneous suppression of pathogenic microorganisms during anticancer chemotherapy could not only interrupt or abolish tumor growth but also eventually protect cancer patients from infection. Hence, the development of novel drugs which exhibit dual anticancer and antibacterial

Received: June 29, 2018
Published: December 3, 2018

DOI: 10.1021/acs.jmedchem.8b01031
J. Med. Chem. 2019, 62, 512−530

Chart 1. Line Drawings of Proligands HL^{1-6} and Cu(II) Complexes $[Cu(L^{1-6})Cl]$ (1−6) Reported in This Work[a]

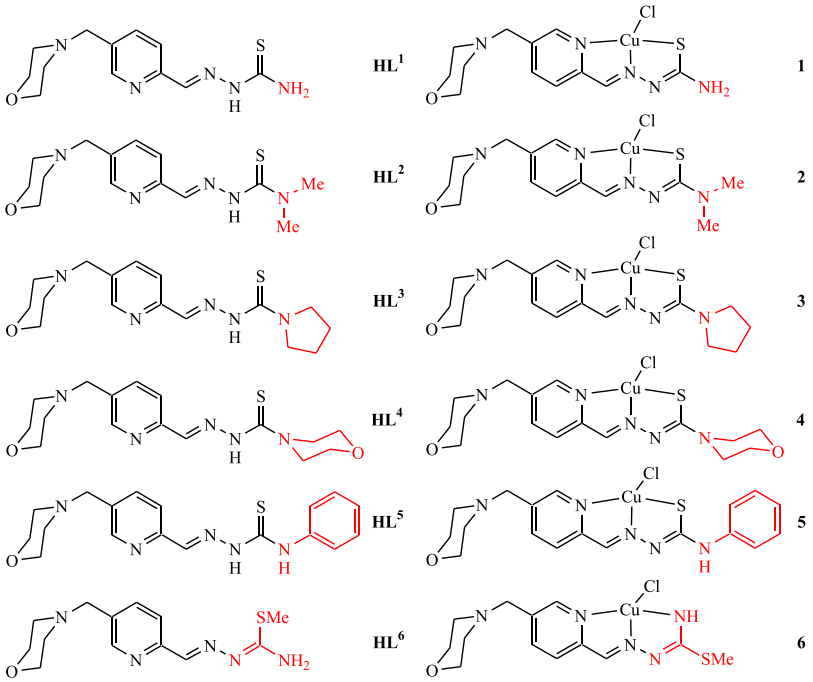

[a]All proligands and Cu(II) complexes, but **HL^3** and **2**, were investigated by single-crystal X-ray crystallography.

properties in comparable concentration range would affect the malignant process and simultaneously decrease the risk of patients' death due to infection, febrile neutropenia, and bacteraemia.

Both cancer and bacterial cells share similar properties, such as high rate of proliferation, rapid adjustment, and quick spreading within the host and aggressive disease progression.[5] To sustain such rapid proliferation, cancer and bacterial cells have to support DNA replication and production of RNA by increasing de novo nucleotide synthesis. Ribonucleotide reductase (RNR) is the key enzyme that catalyzes the reduction of ribonucleotides to their corresponding deoxyribonucleotides, thereby initiating DNA synthesis or repair, making it an important biomolecular target for drugs with anticancer and antibacterial properties.[6,7] RNR consists of a large subunit (NrdA or R1), which contains the allosteric site that regulates and catalyzes substrate reduction, and a small subunit (NrdB or R2) with the diferric-tyrosyl radical cofactor, essential for the catalytic activity of the RNR enzyme. Small molecules, that can sequester Fe from the dinuclear metal center and/or scavenge the tyrosyl radical, inhibit R2 activity, thereby preventing de novo DNA synthesis in cancer cells and bacteria.

α-*N*-Heterocyclic thiosemicarbazones (TSCs) are excellent transition-metal chelators and have a broad range of activities, including anticancer and antibacterial properties, which are believed to be at least partially due to their RNR inhibition.[8] To date, several TSC compounds, namely, 3-amino-2-pyridinecarboxaldehyde TSC (triapine),[9−11] di-2-pyridylketone 4-cyclohexyl-4-methyl-3-thiosemicarbazone (DpC),[12,13] and (*E*)-*N*′-(6,7-dihydroquinolin-8(5*H*)-ylidene)-4-(pyridine-2-yl)piperazine-1-carbothiohydrazide (COTI-2)[14] are undergoing phase I and II clinical trials against various types of cancer. The main caveat in the use of TSCs is their high toxicity which is reflected in a number of side effects in clinical trials involving triapine.[9−11] Many studies have shown that Cu(II)−TSC complexes often display better selectivity than their TSC proligands, which can be attributed to the induction of different intracellular signaling pathways.[15]

Despite advances in the design and synthesis of new TSCs and Cu(II)−TSC complexes over the years, these compounds are facing the problem of low aqueous solubility, thereby hampering their further development. Therefore, the synthesis of water-soluble and cytotoxic TSCs and Cu(II)−TSC complexes requires a thoughtful selection of the functional groups that can be attached at the TSC backbone without reducing their biological activity.[16−20] With the aim to reach the optimal combination of aqueous solubility and high cytotoxicity, we designed new (iso)TSC−morpholine hybrids and their Cu(II) complexes. Notably, morpholine moiety was chosen because it confers excellent water solubility, which typically translates into an improved pharmacological effect. Additionally, morpholine derivatives possess a broad spectrum of biological activities, including anticancer and antibacterial therapeutic potential.[21] For example, commercial anticancer drugs aprepitant and gefinitib, as well as antibacterial drugs finafloxacin and levofloxacin include a morpholine fragment in their structures.

Herein, we report on the synthesis of water-soluble proligands **HL^{1-6}** and Cu(II) complexes **1−6** (Chart 1), which were characterized by analytical and various spectroscopic techniques. X-ray diffraction structures of **HL^1**, **HL^2**, **HL^4−HL^6**, and **1**, **3−6** were established, and solution equilibria studies for **HL^1** and Cu(II) complex formation with **HL^1** by pH-potentiometry, UV−vis, electron paramagnetic resonance (EPR), and ^{1}H NMR spectroscopy, as well as electrochemistry, were performed. Antiproliferative activity against human ovarian cancer A2780 and cisplatin resistant A2780cis cell lines, noncancerous HEK293 cell line, as well as antibacterial activity against Gram-positive (*Staphylococcus aureus*) compared with Gram-negative bacteria (*Pseudomonas aeruginosa*) were investigated and structure−

DOI: 10.1021/acs.jmedchem.8b01031
J. Med. Chem. 2019, 62, 512−530

Scheme 1. Synthesis of 5-Methylmorpholine-pyridine-2-carboxaldehyde[a]

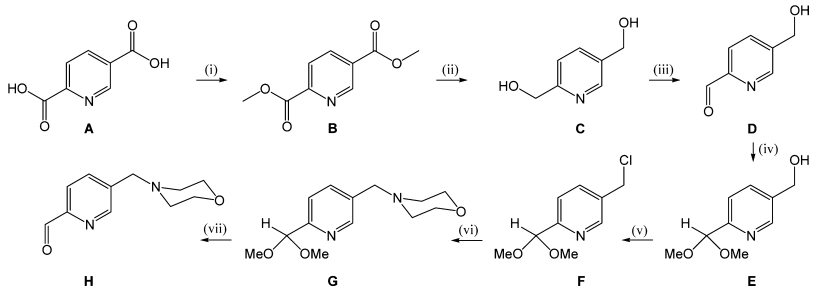

[a]Reagents and conditions: (i) thionyl chloride, methanol, 0 °C → room temperature, 12 h;[22] (ii) sodium borohydride, ethanol, acetone, potassium carbonate, chloroform, 0 °C, 1 h → reflux, overnight;[23] (iii) selenium dioxide, dioxane, water, 100 °C, 3 h;[24] (iv) trimethyl orthoformate, methanesulfonic acid, methanol, reflux, 48 h; (v) thionyl chloride, dichloromethane, −80 °C → room temperature, overnight; (vi) moprholine, triethylamine, tetrahydrofuran/CH_2Cl_2 1:1, 50 °C, overnight, purification by column chromatography; and (vii) HCl, water, 60 °C, overnight.

activity relationships were discussed. The processes controlling cellular accumulation of **2** were investigated. Preliminary insights into the mode of action of **2** and **5**, including mouse R2 RNR inhibitory potential, studied by molecular modeling and tyrosyl radical quenching monitored by EPR spectroscopy, as well as by western blotting and flow cytometry, are also presented.

2. RESULTS

2.1. Synthesis and Characterization of (Iso)TSC−Morpholine Hybrids and Their Cu(II) Complexes. The 5-methylmorpholine-pyridine-2-carboxaldehyde **H** was prepared in seven steps as shown in Scheme 1, and the detailed synthesis is described in the Supporting Information. First, pyridine-2,5-dicarboxylic acid **A** was converted into diester **B** that was further reduced to the diol **C**. The latter was selectively oxidized with SeO_2 to the aldehyde **D**. After protection of the aldehyde group, the alcohol **E** was converted into the chloride **F** that was further reacted with morpholine to give species **G**. Finally, the hydrolysis of the methyl ester function in acidic conditions afforded the required aldehyde **H** for condensation reactions with thiosemicarbazide, 4*N*-dimethyl-3-thiosemicarbazide, 4*N*-pyrrolydinyl-3-thiosemicarbazide, 4*N*-morpholinyl-3-thiosemicarbazide, 4*N*-phenyl-3-thiosemicarbazide, and *S*-methylisothiosemicarbazide hydroiodide to give the hybrids $\mathbf{HL^{1-6}}$ (Chart 1), respectively. One- and two-dimensional NMR spectra were in agreement with the proposed structures for $\mathbf{HL^{1-6}}$, enabling the assignment of all ^1H and ^{13}C resonances. The ESI mass spectra recorded in a positive ion mode showed strong peaks corresponding to $[M + H]^+$ and $[M + Na]^+$ ions, respectively. The proligands $\mathbf{HL^{1-6}}$ were reacted with Cu(II) chloride dihydrate and triethylamine in 1:1:1 mole ratio in methanol to give $[\mathbf{Cu(L^{1-6})Cl}]$ (**1**−**6**) in 35−91% yields (Chart 1). Positive ion ESI mass spectra showed strong peaks attributed to $[Cu(L^{1-6})]^+$ ions. The structures of **1**, **3**−**6** were also established by single-crystal X-ray diffraction (vide infra).

2.2. X-ray Crystallography. The results of X-ray diffraction studies of $\mathbf{HL^1}$, $\mathbf{HL^2}$, and $\mathbf{HL^{4-6}}$ are shown in Figure S1, whereas those of $[\mathbf{Cu(L^1)Cl}]$ (**1**), $[\mathbf{Cu(L^3)Cl}]$ (**3**), $[\mathbf{Cu(L^4)Cl}]$ (**4**), $[\mathbf{Cu(L^5)Cl}]$ (**5**), and $[\mathbf{Cu(L^1)Cl(H_2O)}]$ (**1′**), $[\mathbf{Cu(L^6)Cl}]$ (**6**) are shown in Figures 1 and 2, respectively. Selected bond distances and bond angles are quoted in Tables S1 and S2. The proligands adopted different isomeric configurations in the solid state depending on substituents at the terminal nitrogen atom of the thiosemicarbazide moiety. Complexes **1**, **3**, **4**, and **5** form dimeric associates as shown in Figure 1 (co-crystallized solvent was omitted for clarity). Each Cu(II) ion has a distorted square-planar coordination geometry. Intermolecular contacts supporting the dimeric associates in the crystals are of different nature in **1** and **3**−**5**, respectively. The presence of long intermolecular contacts Cu···Cl or Cu···Cl and Cu···S (see legend to Figure 1) provides evidence of weak association of complexes in dimers, which most probably dissociate in solution with formation of monomeric species. There was no evidence from ESI mass spectra on the presence of dimeric species in solution.

Moreover, $\mathbf{HL^1}$ reacts with $CuCl_2$ in aqueous solution with formation of five-coordinate complex $[\mathbf{Cu(L^1)Cl(H_2O)}]$ (**1′**·$2H_2O$) (Figure 2a). The monomeric square-planar complex $[\mathbf{Cu(L^6)Cl}]$ forms an infinite chain via weak coordination of the morpholine oxygen atom of one complex to the Cu(II) atom of the next molecule as shown in Figure S2. The intermolecular Cu···O contact is of 2.603(3) Å.

2.3. Solution Chemistry. To establish the presence of isomers of the proligands in aqueous solution and proton dissociation processes, in which these can be involved, solution equilibrium studies have been performed. Likewise, the solution speciation of the copper(II) complexes, as well as their stability have been investigated to elucidate the species, which is the most stable and abundant at physiological pH. The proligand $\mathbf{HL^1}$ (Chart 1) was chosen for the detailed solution equilibrium studies because it has the simplest structure and the best aqueous solubility among the proligands prepared. The presence of different isomers in solution was excluded by measurements of ^1H NMR spectra in 10% D_2O/90% H_2O (Figure S3), which showed only one set of signals for the proligand in accordance to its low (C_1) molecular symmetry. The proligand most probably adopts the *E* configuration found in the solid state (Figure S1). The same configuration was reported previously for the reference compound 2-formylpyridine thiosemicarbazone in polar solvents.[25] Proton dissociation processes were monitored in aqueous solution by pH-potentiometric and ^1H NMR titrations and three pK_a values were determined by both methods (Table S3). According to the obtained pK_a values, $\mathbf{HL^1}$ is mainly neutral (97% HL, 3% H_2L^+) at physiological pH (Figure S4). Inspection of ^1H NMR spectra revealed stepwise deprotonation of three functional groups in the following order: $N_{pyridinium}H^+ \rightarrow N_{morpholinium}H^+ \rightarrow N_{hydrazine}H$ (Figure S3).

DOI: 10.1021/acs.jmedchem.8b01031
J. Med. Chem. 2019, 62, 512−530

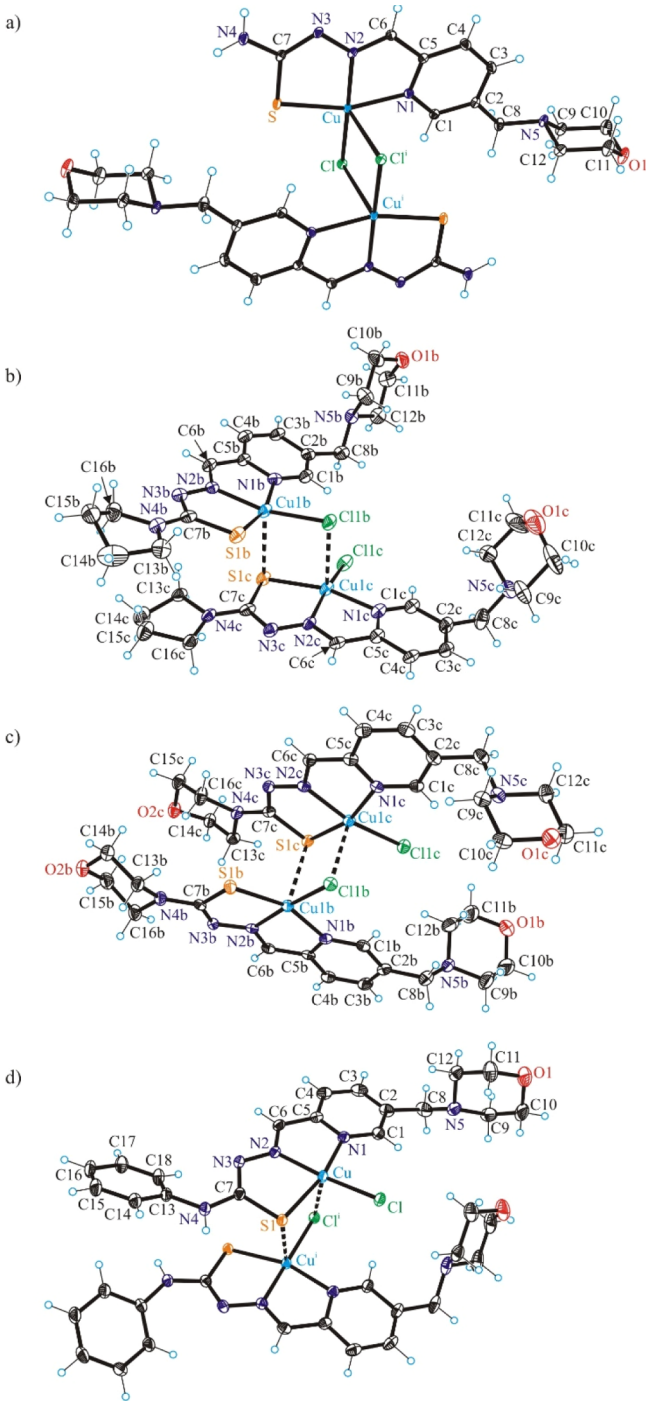

Figure 1. ORTEP views of weak dimeric associates of (a) $[Cu(L^1)Cl]$ (**1**), (b) $[Cu(L^3)Cl]$ (**3**), (c) $[Cu(L^4)Cl]_2$ (**4**), and (d) $[Cu(L^5)Cl]$ (**5**).

The solution speciation of the Cu(II) complexes with HL^1 was characterized by the combined use of pH-potentiometry, UV−vis spectrophotometry [via charge transfer (CT) and d−d bands], and EPR spectroscopy. The spectral changes (Table S4, Figures 3a and S5) in the UV and visible regions measured at 1:1 metal-to-ligand ratio show the high-extent formation of a Cu(II) complex already at strongly acidic pH values (e.g., pH 1) and its stepwise deprotonation by increasing the pH. At pH 7.4, the dominant species is $[CuL]^+$ (Figure 3b).

Because of the high stability of the Cu(II) complexes formed, the cumulative constant ($\log \beta$) for the $[CuL]^+$ species

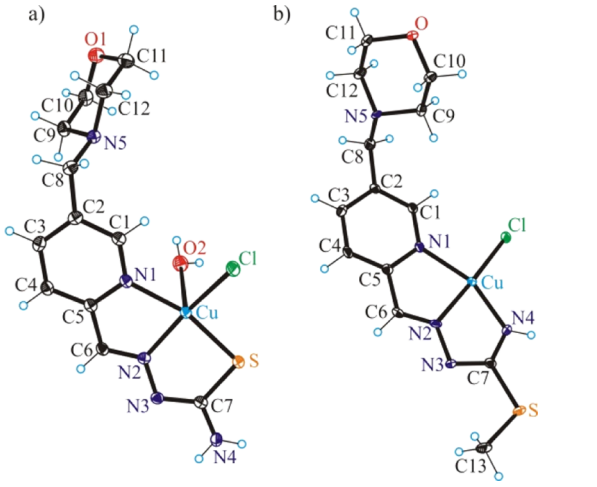

Figure 2. ORTEP views of (a) $[Cu(L^1)Cl(H_2O)]$ (**1′**) and (b) $[Cu(L^6)Cl]$ (**6**).

(Table S4) was determined via ethylenediaminetetraacetic acid (EDTA) displacement studies (Figure S6). Then, the pK_a and the log β values for the other type of complexes ($[CuLH_2]^{3+}$, $[CuLH]^{2+}$, $[CuLH_{-1}]$) were computed using each method, and data were in a fairly good agreement (Table S4). It is worth noting that formation of a bis-ligand complex $[CuL_2]$ at ligand excess was also confirmed by the UV−vis CT and EPR titrations. The d−d bands (Figure S5) recorded from pH 3.4 to 7.5 at 1:1 metal-to-ligand ratio revealed that the proton dissociation process of $[CuLH]^{2+} \rightarrow [CuL]^+$ is accompanied by rather weak spectral changes as most probably the noncoordinating morpholinium NH^+ is deprotonating. To further characterize, the coordination modes of the various complexes in solution EPR parameters (Table S5) obtained by the deconvolution of the recorded spectra (Figure S7) were analyzed. The isotropic g and A values of $[CuLH]^{2+}$ and $[CuL]^+$ are quite similar, indicating the like coordination mode.

Comparison of the EPR parameters of the Cu(II) complexes of HL^1 with those of 2-formylpyridine thiosemicarbazone[25] and triapine[26] permitted to conclude that in the $[CuLH]^{2+}$ and $[CuL]^+$ complexes a typical coordination mode via the $N_{pyridyl}$, N, S^- binding site is realized in accordance with the X-ray diffraction data. $[CuLH_2]^{3+}$ contains the diprotonated ligand in which the protons are attributed to the noncoordinating N^2H and morpholinium NH^+ moieties, while $[CuLH_{-1}]$ is most probably a mixed hydroxido complex $[CuL(OH)]$ formed by the deprotonation of water molecule coordinated in the fourth equatorial position. At ligand excess besides the bis-ligand complex, a minor dinuclear species $[Cu_2L_3H]^{2+}$ was detected resulting in the weak exchange coupling between neighboring Cu(II) centers smearing out the expected hyperfine structure.

2.4. Cu(II)−TSC Complexes Undergo Quasi-Reversible One-Electron Reduction at Biologically Accessible Potentials. To assess the redox properties of **1**−**6**, detailed electrochemical and spectroscopic studies in various solvents were performed using cyclic voltammetry as well as EPR-spectroelectrochemistry. Additionally, the UV−vis spectra of **1**−**5** were measured (Figure S8). Electrochemical and spectroscopic data are summarized in Table S6. Almost reversible one-electron cathodic reduction was observed for **1**−**5** in dimethyl sulfoxide (DMSO) with half-wave redox potentials from −0.77 to −0.81 V versus Fc^+/Fc [for

DOI: 10.1021/acs.jmedchem.8b01031
J. Med. Chem. 2019, 62, 512−530

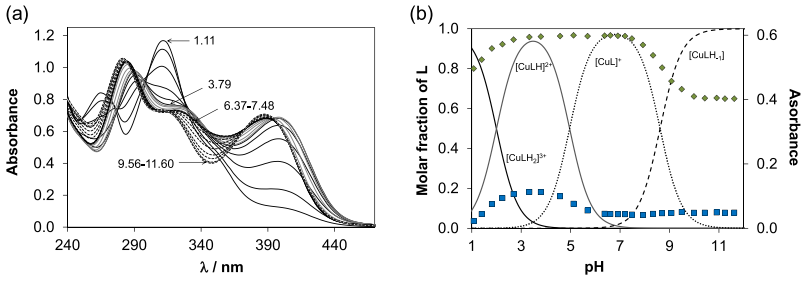

Figure 3. UV−vis spectra recorded for the Cu(II)−**HL**[1] (1:1) system at various pH values (a), and concentration distribution curves and measured absorbance values at 346 nm (♦) and 440 nm (■) for the same system (b). {$c_{Cu(II)} = c_{lig}$ = 121 μM; T = 298 K; I = 0.10 M (KCl); l = 0.5 cm}.

comparison from −0.13 to −0.17 V vs normal hydrogen electrode (NHE)] (Table S6 and Figure S9). In general, the values of redox potentials of **1**−**6** for the first reduction step decreased in the following rank order ($E_{1/2}$(**5**) > $E_{1/2}$(**2**) = $E_{1/2}$(**3**) = $E_{1/2}$(**4**) > $E_{1/2}$(**1**) > $E_{1/2}$(**6**)). The second reduction step occurred at −1.8 V versus Fc^+/Fc (−1.16 V vs NHE) and was less reversible, indicating a ligand-based reduction. This was confirmed by the CVs of the corresponding proligands which exhibited the first reduction step at around −1.9 V versus Fc^+/Fc (not shown). In aqueous solutions, the reduction potentials shifted to the less negative values, and reduction was less reversible as shown for **2** in Figure S10. Complex **6** exhibited different redox behavior with the lowest electrochemical reversibility and the most negative reduction potential of −0.86 V versus Fc^+/Fc (−0.26 V vs NHE) (Figure S9c). Unlike the cathodic reduction, the anodic oxidation of **1**−**6** was irreversible with potential values in the region from 0.4 to 0.8 V versus Fc^+/Fc (0.68 V to 1.44 V vs NHE). A similar response was observed for the corresponding proligand **HL**[2] (Figure S11), indicating ligand based oxidation in **2**.

2.5. Biologically Accessible Reduction of Cu(II)−TSC Complexes is Cu-Centered. To investigate whether the biologically accessible reduction is metal-centered, the reversible one-electron reduction of **5** was further studied by in situ UV−vis-spectroelectrochemistry (Figure 4a). Upon cathodic reduction at the first reduction peak, two isosbestic points at 389 and 325 nm were detected. The spectral changes of the S → Cu(II) CT bands (~425 nm) clearly confirmed the reduction of Cu(II) to Cu(I). Additionally, upon voltammetric reverse scan, reoxidation and a nearly full recovery of the initial optical bands were observed, attesting the chemical reversibility of the cathodic reduction even at low scan rates (Figure 4). To confirm the involvement of Cu(II) in the reduction processes, in situ EPR electrochemistry of **1**−**6** in nBu$_4$NPF$_6$/DMSO and water was performed because metal-based reduction would result in the formation of EPR-silent Cu(I) species (Figure 4b). As can be seen for electrochemical reduction of **2** in nBu$_4$NPF$_6$/DMSO in the region of the first one-electron reduction step (see inset in Figure 4b), a significant decrease of EPR signal was observed in accord with the formation of a diamagnetic Cu(I) d^{10} complex. For aqueous solutions, the reversibility was significantly reduced, implying a more complex mechanism involving the release of the proligand. However, by decreasing the scan rate and going to the more positive potentials upon reverse scan, a partial recovery of the initial optical bands was also observed in aqueous solutions as shown for **2** in Figure S12. Thus, electrochemical data indicated a likely reduction of Cu(II)−TSC complexes to Cu(I) species with the subsequent release of the proligands.

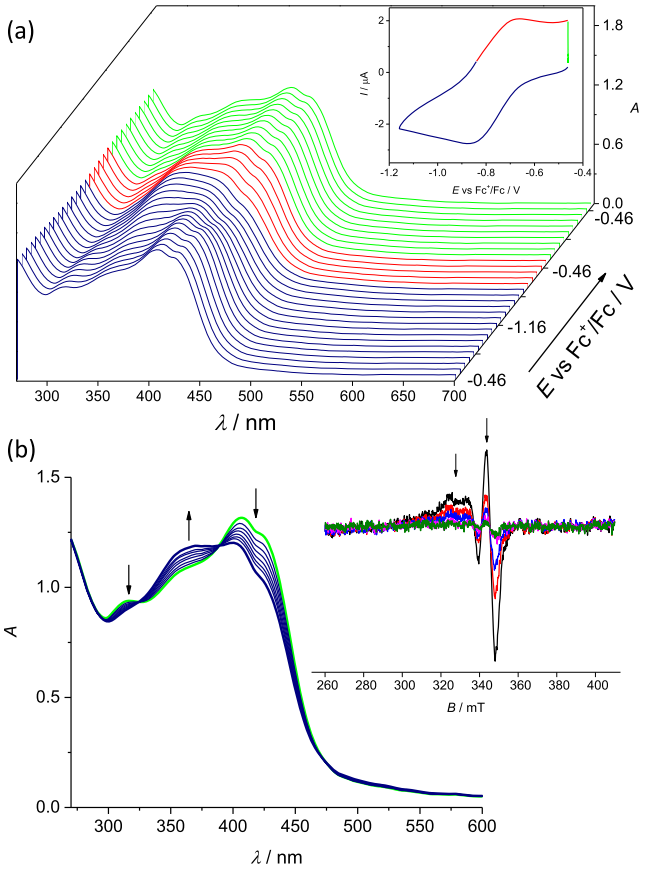

Figure 4. Spectroelectrochemistry of **2** in nBu$_4$NPF$_6$/DMSO in the region of the first cathodic peak. (a) Potential dependence of UV−vis spectra with respective cyclic voltammogram (Pt-microstructured honeycomb working electrode, scan rate v = 5 mV s^{-1}); (b) evolution of UV−vis spectra in 2D projection in forward scan (inset: EPR spectra measured at the first reduction peak using Pt mesh working electrode).

2.6. Lead TSCs and Their Cu(II) Complexes Exhibited Marked Antiproliferative Activity in a Nanomolar Concentration Range. The in vitro anticancer activity of **1**−**6** and their respective TSCs was determined in ovarian carcinoma cells (A2780 and A2780cisR) and noncancerous human embryonic kidney cells (HEK293) by the colorimetric MTT assay with an exposure time of 72 h. The IC_{50} values for **HL**[1]−**HL**[6] and **1**−**6** in comparison with triapine, $CuCl_2$, Cu-triapine and cisplatin are listed in Tables 1 and 2, respectively, and concentration−effect curves are depicted in Figure S13.

With the exception of **HL**[1] and **HL**[6], the proligands demonstrated marked antiproliferative activity in a submicro-

DOI: 10.1021/acs.jmedchem.8b01031
J. Med. Chem. 2019, 62, 512−530

Table 1. Cytotoxicity of Proligands HL^{1-6} and Their *n*-Octanol/Water Distribution Coefficients (log $D_{7.4}$)

compound	IC_{50} [μM][a] A2780	A2780cis	RF[b]	HEK293	SF[c]	log $D_{7.4}$[d]
HL^1	7.6 ± 1.9	13 ± 1	1.7	9.1 ± 1.7	1.2	+0.46 ± 0.01
HL^2	0.010 ± 0.001	0.035 ± 0.006	3.5	0.030 ± 0.005	3.0	+0.51 ± 0.02
HL^3	0.008 ± 0.002	0.028 ± 0.006	3.5	0.022 ± 0.005	2.8	+1.0 ± 0.1
HL^4	0.07 ± 0.01	0.76 ± 0.06	10.9	0.35 ± 0.05	5.0	+0.37 ± 0.04
HL^5	0.31 ± 0.08	1.1 ± 0.2	3.5	0.67 ± 0.06	2.2	≥2
HL^6	157 ± 21	426 ± 44	2.7	89 ± 2	0.6	+0.84 ± 0.01
triapine	0.67 ± 0.22	1.1 ± 0.1	4.6	0.39 ± 0.05	0.6	n.d.[e]

[a]50% inhibitory concentrations (IC_{50}) in human ovarian carcinoma cell lines A2780 and A2780cisR and human embryonic kidney cell line HEK293, determined by the MTT assay after 72 h exposure. Values are means ± standard deviations (SDs) obtained from at least three independent experiments. [b]Resistance factor (RF) is determined as $IC_{50(A2780cisR)}/IC_{50(A2780)}$. [c]Selectivity factor (SF) is determined as $IC_{50(HEK293)}/IC_{50(A2780)}$. [d]Distribution coefficients for *n*-octanol and buffered aqueous solution determined at physiological pH by UV−vis spectroscopy. Values are means ± SDs obtained from at least three independent experiments. [e]n.d.—not determined.

Table 2. Cytotoxicity of Cu(II)−TSC Complexes 1−6, $CuCl_2$ and Cisplatin and Their *n*-Octanol/Water Distribution Coefficients (log $D_{7.4}$)

compound	IC_{50} [μM][a] A2780	A2780cis	HEK293	RF[b]	SF[c]	cellular accumulation,[d] nmol Cu/mg protein A2780	log $D_{7.4}$[e]
1	2.2 ± 0.1	13 ± 4	16 ± 2	5.9	7.3	0.63 ± 0.09	−0.81 ± 0.04
2	0.012 ± 0.002	0.030 ± 0.003	0.032 ± 0.008	2.5	2.7	3.9 ± 0.6	+0.30 ± 0.01
3	0.26 ± 0.02	0.60 ± 0.05	0.78 ± 0.20	2.3	3.0	2.2 ± 0.6	+0.86 ± 0.02
4	0.08 ± 0.01	0.26 ± 0.04	0.24 ± 0.02	3.3	3.0	3.2 ± 0.7	+0.12 ± 0.01
5	0.009 ± 0.002	0.017 ± 0.002	0.020 ± 0.003	1.9	2.2	4.1 ± 0.9	+1.49 ± 0.06
6	43 ± 3	62 ± 6	72 ± 0	1.4	1.7	0.47 ± 0.08	−0.23 ± 0.01
$CuCl_2$	83 ± 12	82 ± 3	187 ± 37	1.0	2.3	0.17 ± 0.05[f]	n.d.[g]
Cu-triapine[h]	1.3 ± 0.1	29 ± 0.3	n.d.	22.3	–	n.d.	n.d.
cisplatin	0.44 ± 0.13	4.6 ± 0.3	n.d.	10.5	–	–	−2.30 ± 0.79[i]

[a]50% inhibitory concentrations (IC_{50}) in human ovarian carcinoma cell lines A2780 and A2780cisR and human embryonic kidney cell line HEK293, determined by the MTT assay after exposure for 72 h. Values are means ± SDs obtained from at least three independent experiments. [b]RF is determined as $IC_{50(A2780cisR)}/IC_{50(A2780)}$. [c]SF is determined as $IC_{50(HEK293)}/IC_{50(A2780)}$. [d]Cellular accumulation in A2780 cells, determined by Inductively Coupled Plasma Mass Spectrometry (ICP−MS) after 24 h exposure at concentration of 1 μM. Values are means ± SDs obtained from at least three independent experiments. [e]Distribution coefficients for *n*-octanol and buffered aqueous solution determined at physiological pH by UV−vis spectroscopy. Values are means ± SDs obtained from at least three independent experiments. [f]Cellular accumulation of $CuCl_2$ was detected at concentration of 2.5 μM. [g]n.d.—not determined. [h]The IC_{50} values (exposure for 72 h) were taken from the ref 27. [i]log $P_{o/w}$ value was taken from the ref 28.

molar to nanomolar concentration range in both A2780 and A2780cisR cells. The efficacy of compounds HL^2, HL^3, and HL^5 in cisplatin-resistant A2780cisR cells decreased by factor 3.5 in comparison to that in sensitive A2780 cells, whereas a 4.6- and 11-fold drop of activity was observed for triapine and HL^4, respectively. The activity of proligands HL^{1-6} and triapine increased in the following rank order $HL^6 < HL^1 <$ **triapine** $< HL^5 < HL^4 \ll HL^2 \approx HL^3$ (Table 1).

As can be seen in Table 2, with the exception of **3**, all Cu(II)−TSC complexes were equally or more cytotoxic than the respective proligands. The activity of complexes **1**−**6** increased in the following order **6** < **1** < **3** < **4** ≪ **2** < **5**, similar to the trend in electrochemical redox potentials for Cu-based reduction step (Table S6). To compare the cytotoxicity of **1**−**6** with that of $[Cu(H_2O)_6]^{2+}$, A2780 cells were treated with aqueous solution of $CuCl_2$. In agreement with the literature,[29] $CuCl_2$ revealed antiproliferative activity in the high micromolar range, in contrast to high activity of **1**−**6**, which should be regarded as individual entities with their own biological, pharmacokinetic, and metabolic profiles. Complexes **1**−**6** were up to ∼50 times more cytotoxic than cisplatin in A2780 cells and up to ∼270 times more cytotoxic in A2780cisR cells. Additionally, the differences in cytotoxicity of **1**−**6** in A2780 and A2780cisR cells were significantly lower than that for HL^1−HL^6 and cisplatin, indicating high potential of Cu(II) complexes for the treatment of cisplatin-resistant tumors. The most active TSC proligands and their respective Cu(II) complexes were more selective toward A2780 cells over HEK293 cells; however, they did not show any selectivity toward A2780cisR cells over HEK293 cells. On the contrary, triapine was significantly more cytotoxic toward noncancerous HEK cells than A2780 or A2780cis cells.

2.7. Antiproliferative Activity of Cu(II)−TSC Complexes Correlates with Their Cellular Accumulation and Lipophilicity. The ability of anticancer drugs to penetrate biological membranes, tissues, and barriers underlies their biological, pharmacokinetic, and metabolic properties. These properties can be predicted by calculating physicochemical characteristics of drug candidates using molecular descriptors.[30] To estimate if the proligands HL^1−HL^6 and corresponding Cu(II) complexes demonstrate drug-like properties, they were evaluated with main stream molecular descriptors, such as molecular weight, number of hydrogen bond donors and acceptors (HBA), *n*-octanol−water partition coefficient (log *P*), polar surface area, and rotatable bonds. The results are shown in Table S7 in the Supporting Information. On the basis of the calculated physicochemical parameters, we determined if novel compounds belonged to the *drug-like*

DOI: 10.1021/acs.jmedchem.8b01031
J. Med. Chem. 2019, 62, 512−530

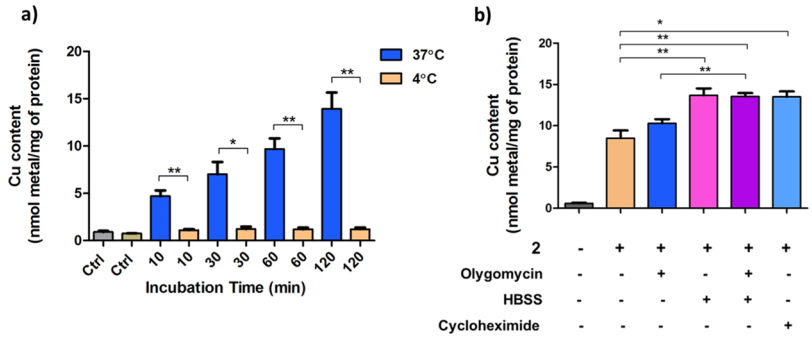

Figure 5. Effects of temperature and inhibitors on the accumulation of **2** in A2780 cells. Intracellular content was determined by ICP−MS: (a) A2780 cells were treated with **2** (3 μM) at 37 or 4 °C for the indicated time periods. (b) A2780 cells were pre-treated with oligomycin (5 μM), and/or pre-incubated in HBSS for 1 h, or pretreated with cycloheximide (100 μM) for 4 h and subsequently co-treated with **2** (3 μM) for 1 h. The presence of inhibitors did not show any effects on the intracellular Cu level of untreated A2780 cells (data not shown). Statistical analysis was performed by two-tailed T-test using GraphPad Prism software (GraphPad Software Inc., CA) with $p < 0.05$ considered as significant (*$p < 0.05$, **$p < 0.01$).

chemical space, which is commonly defined by the well-known Lipinski rule, or to the known drug space (KDS), which includes all small compounds in medical use.[31] As can be seen from Table S7, all compounds fell within the boundaries of *drug-like* chemical space with the exception of **HL^4** which demonstrated higher HBA value, referring to KDS space. On the basis of these results, novel compounds are expected to be sufficiently cell permeable. Following the calculations, we determined the lipophilicity of all compounds experimentally (log $D_{7.4}$, Tables 1 and 2). It is known that cancer cells accumulate hydrophilic compounds to a smaller extent relative to hydrophobic compounds, thereby affecting their activity. Hence, the differences in the lipophilicity of compounds might be related to the observed trends in cytotoxicity of **1**−**6**. In general, with the exception of morpholine derivative **HL^4**, proligands which were obtained by systematic substitution at the terminal thioamide nitrogen demonstrated higher lipophilicity when compared with that of **HL^1**. As expected, proligands were more lipophilic than the corresponding Cu(II) species, which are positively charged at physiological pH (Figure 3b). Among Cu(II)−TSC complexes, only the least cytotoxic complexes **1** and **6**, as well as cisplatin, demonstrated negative log $D_{7.4}$ values, indicating their higher hydrophilicity. The lipophilicity of **2**−**5** increased in the following order **4** < **2** < **3** < **5**, and correlated well with their cytotoxicity in cancer cells, with the exception of **3**. Subsequently, we determined the total cellular accumulation of Cu in A2780 cells by ICP−MS upon 24 h exposure to **1**−**6** in comparison with $CuCl_2$ (Table 2). The IC_{50} values from MTT assays with 72 h drug exposure varied from nanomolar to high micromolar concentrations; therefore, in the cellular accumulation experiment cells were treated with 1 μM of compounds of interest for 24 h to minimize cell detachment. The cellular accumulation of all Cu(II)−TSC complexes was significantly higher than for $CuCl_2$, indicating the role of lipophilic TSC ligands in the delivery of the complexes into the cells. The accumulation increased in the order **6** < **1** < **3** < **4** < **2** < **5**.

2.8. Cellular Accumulation and Efflux of Cu(II)−TSC Complexes are Energy- and/or Temperature-Dependent Processes. Dependence of cytotoxicity on lipophilicity of **1**−**6** indicates that their cellular accumulation at least partially occurs via passive diffusion. In order to gain additional insights into the mechanisms controlling the accumulation of Cu(II)−TSC complexes, we investigated the effects of temperature and various inhibitors on total cellular accumulation of **2** with the results shown in Figure 5. A2780 cells were treated with **2** at 3 μM for 30, 60 and 120 min at 37 and 4 °C and intracellular Cu content was measured by ICP−MS. Prolonged incubation at low temperatures may result in the changes in membrane fluidity, decreasing membrane permeability and restricting drug uptake;[32] therefore, the shorter time point of 10 min was also included. The cellular accumulation of **2** dramatically decreased at low temperature even after 10 min treatment, indicating the involvement of active carrier-mediated transport or facilitated diffusion. Likewise, the decrease of cellular accumulation at low temperatures has been reported for both Cu(II)−TSC complexes and metal-free TSCs.[33,34] To further clarify whether the uptake of **2** requires energy, the cellular ATP production was blocked by incubating cells in a saline solution [Hank's Balanced Salt Solution (HBSS)], resulting in total starvation and rapid reduction of intracellular ATP content, and/or by addition of oligomycin, leading to the inhibition of oxidative phosphorylation.

When A2780 cells were pretreated with 5 μM of oligomycin for 1 or 4 h and subsequently co-treated with 3 μM of **2**, the intracellular Cu levels were not affected, even though the mitochondrial respiration of the cancer cells was successfully inhibited (data not shown). However, when A2780 cells were starved in HBSS for 1 h and subsequently treated with 3 μM of **2** for 1 h, an increase in intracellular Cu content was observed. Co-treatment of **2** with 5 μM of oligomycin in HBSS did not result in a further increase of intracellular Cu levels. The increase of the Cu content in HBSS-starved cells might stem from the inhibition of energy-dependent efflux processes. To assess the role of proteins in both cellular accumulation and efflux of **2**, A2780 cells were pretreated with cycloheximide, which is a known inhibitor of protein synthesis. Significant increase of intracellular Cu content was observed, similar to HBSS starvation, providing further evidence for the involvement of protein-dependent efflux processes. Similar effects have been reported for related Cu(II)−TSC complexes.[33] The data provide evidence that cellular accumulation of **2** occurs via carrier-facilitated diffusion, which might co-exist with passive permeation through the lipid bilayer.[35] The efflux processes, however, are actively mediated by proteins and upon inhibition of protein synthesis or energy production a strong increase of intracellular Cu concentration was observed.

DOI: 10.1021/acs.jmedchem.8b01031
J. Med. Chem. 2019, 62, 512−530

2.9. Cu(II)−TSC Complexes Demonstrated High Antibacterial Activity Against *S. aureus* in a Comparable Concentration Range to Ciprofloxacin. The antibacterial activity of HL^1−HL^6 and **1**−**6** on planktonic cells of *P. aeruginosa* and *S. aureus* was investigated by determination of minimal inhibitory concentration $(MIC)_{50}$ and MIC_{100} values (Table 3). Overall, compounds showed a higher antimicrobial activity against Gram-positive (*S. aureus*) compared with Gram-negative bacteria (*P. aeruginosa*). The highest activity against *S. aureus* was observed for **2**−**5**, which specifically inhibited its growth with MIC_{50} values ranging between 2 and 5 μg/mL and completely abolished its growth at 10 μg/mL (MIC_{100}). This activity is comparable but slightly lower than the antibacterial activity of a well-known benchmarked antibiotic ciprofloxacin (CPX). On the contrary, *P. aeruginosa* exhibited high resistance to most of the compounds tested with the exception of HL^2 and **2** with MIC_{50} values at 70 and 50 μg/mL, respectively.

Compounds HL^6 and **6** based on S-methylisothiosemicarbazide were completely devoid of antibacterial activity and no inhibition of bacterial growth was observed at the whole concentration range tested. Interestingly, metal-free TSCs HL^1−HL^5 displayed relatively low antibacterial activity (MIC_{100} > 300 μg/mL), which was significantly enhanced upon coordination to Cu(II). Subsequently, the mode of action of the most active compounds **2**−**5** was evaluated in *S. aureus* and *P. aeruginosa* using the Live/Dead viability assay. As shown in Figure 6, compounds **2**−**5** greatly reduced cell replication, reflected by the lower number of cells compared with the untreated sample and high percentage of propidium iodide (PI)-stained cells, indicating compromised cell membrane allowing the penetration of PI and a bacteriostatic action of these compounds.

Table 3. Antibacterial Activity of HL^{1-6} and 1−6[a]

	S. aureus (μg/mL)		*P. aeruginosa* (μg/mL)	
	MIC_{50}	MIC_{100}	MIC_{50}	MIC_{100}
HL^1	100	>400	NA	NA
HL^2	10	400	50	100
HL^3	10	300	100	NA
HL^4	100	>400	NA	NA
HL^5	10	300	NA	NA
HL^6	NA	NA	NA	NA
1	100	>500	NA	NA
2	2	10	70	200
3	3	10	100	400
4	5	10	100	400
5	3	10	200	450
6	NA	NA	200	NA
CPX	0.5	1	0.5	2

[a]See Experimental Section for details. NA denotes no antibacterial activity detected (>500 μg/mL).

2.10. TSCs and Their Cu(II) Complexes Are Located in a Close Proximity to the Active Site of Mouse R2 RNR Protein. Next, the RNR inhibitory potential of the TSC proligands HL^1−HL^6 and their corresponding Cu(II) complexes **1**−**6** was investigated. The proligands HL^1−HL^6 and Cu(II) complexes **1**−**6** were docked into the crystal structure of mouse R2 RNR subunit (PDB ID: 1W68)[36] using GOLD software.[37] To predict the binding of **1**−**6**, the GoldScore function was used and its parameters were modified to include Cu because they are not in GOLD's database.[38] The results of the scoring functions are presented in Table S8. Overall, similar docking results were observed for all proligands and their Cu(II) complexes, suggesting a plausible binding to the mouse R2 protein. The compounds were deeply embedded into the pocket of the R2 subunit, close to the diferric center (Fe_2O), and the enzymatically essential tyrosyl residue (Tyr177). The docked configuration of **5** in comparison with triapine into the binding site is shown in Figure 7. An overlap with triapine was predicted, resulting in a partial reproduction of a hydrogen-bonding pattern (Figure S14, Table S8).

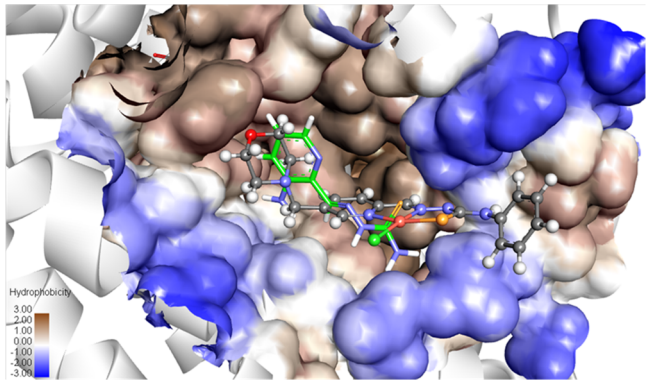

Figure 7. Overlay of docked configurations of Cu(II) complex **5** (gray) and triapine (green) in the binding site of the mouse R2 RNR protein (PDB ID: 1W68). The surface is rendered. Blue and brown depict hydrophilic and hydrophobic areas, respectively.

2.11. Lead TSCs and Their Cu(II) Complexes Cause Moderate Inhibition of a Mouse R2 RNR Protein in a Reducing Environment as a Result of Iron Chelation.

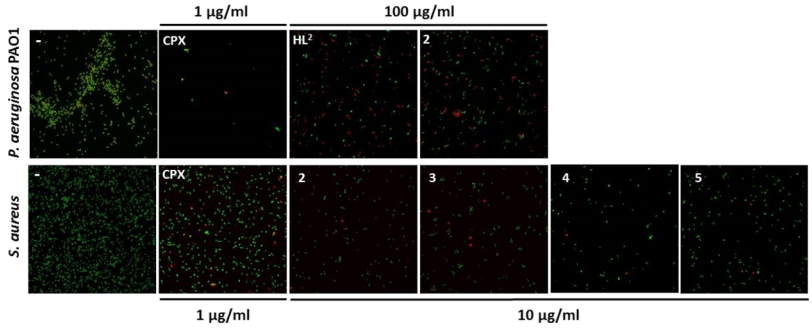

Figure 6. Live/dead bacterial cells are shown by staining with green fluorescence indicating live cells and red fluorescence indicating dead cells.

DOI: 10.1021/acs.jmedchem.8b01031
J. Med. Chem. 2019, 62, 512−530

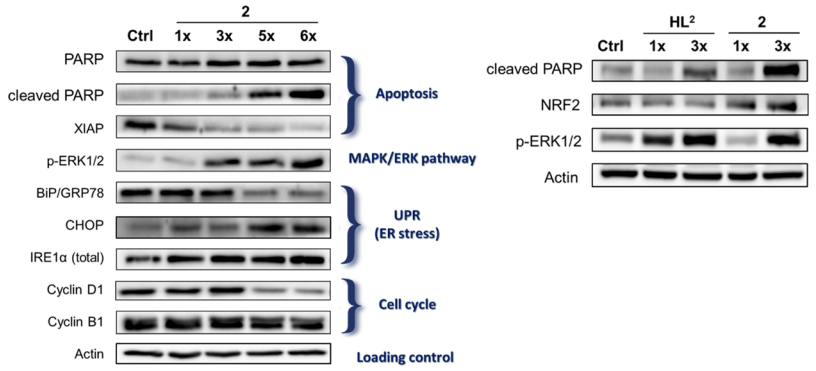

Figure 8. Western blot analysis of various proteins. A2780 cells were treated with increasing concentrations of proligand **HL**^{2} and complex **2** (corresponding to IC_{50} value from MTT experiment with exposure time of 72 h) for 24 h. Total lysates were isolated and examined by Western blot. Actin was used as a loading control.

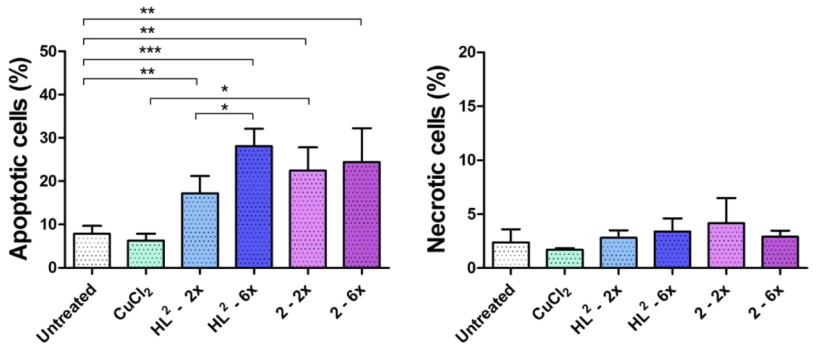

Figure 9. Bar graphs showing the percentage of cell death due to apoptosis (left) and necrosis (right) in A2780 cells treated with increasing concentrations of **HL**^{2}, **2** ($2IC_{50}$ and $6IC_{50}$) and $CuCl_2$ and detected by Annexin V/PI apoptosis assay. Statistical analysis was performed by two-tailed *T*-test using GraphPad Prism software (GraphPad Software Inc., CA) with $p < 0.05$ considered as significant ($^*p < 0.05$, $^{**}p < 0.01$).

The effects of the most cytotoxic complexes **2** and **5**, and the corresponding proligands **HL**^{2} and **HL**^{5}, on the mouse R2 tyrosyl radical were investigated by EPR spectroscopy at 30 K. The proligands and their Cu(II) complexes were incubated with the mouse R2 RNR protein at 1:1 protein-to-compound mole ratio at 298 K in the presence or absence of the reducing agent dithiothreitol (DTT), and the time-dependent reduction of the tyrosyl radical was monitored.[39] Tyrosyl radical reduction by the investigated compounds was observed only in the presence of DTT. Upon incubation with **HL**^{2}, **HL**^{5}, and **2**, **5**, 50% of tyrosyl radical was reduced within 90 s, after which no further reduction was observed (Figure S15). Because the diferric center of the mouse R2 protein is expected to be reduced upon addition of DTT,[40,41] the ability of proligands **HL**^{2} and **HL**^{5} to form stable Fe(II) complexes was investigated by monitoring these reactions by UV−vis measurements in buffered aqueous solutions at pH 7.4. **HL**^{2} and **HL**^{5} (λ_{max} = 312 and 320 nm, respectively) readily reacted with $FeSO_4 \cdot 7H_2O$ affording Fe(II) bis-ligand complexes (λ_{max} = 373, 610 nm and λ_{max} = 385, 645 nm, respectively) at both 1:1 and 1:2 Fe-to-ligand mole ratios. Additionally, the formation of Fe(III) complexes with the subsequent reduction by DTT was investigated (Figure S15). **HL**^{2} and **HL**^{5} reacted with $FeCl_3 \cdot 6H_2O$ (at 1:1 or 1:2 Fe-to-ligand mole ratios) to give $[Fe^{III}(L^2)_2]^+$ and $[Fe^{III}(L^5)_2]^+$ complexes (λ_{max} = 378 nm, 612 nm and λ_{max} = 386 nm, 635 nm, respectively). The formation of $[Fe^{III}(L^5)_2]^+$ species was confirmed by ESI-MS (Figure S16). The absorption spectra of reduced forms were almost identical to those of Fe(II) bis-ligand species and to the previously reported spectra of other Fe^{II}−TSC complexes.[42]

2.12. HL^2 and 2 Induced Unfolded Protein Response, Antioxidant Defense, and Cell Cycle Perturbations. To get further insights into the mechanism of action of **2**, Western blotting of endoplasmic reticulum (ER) stress-related protein markers, namely, IRE1α, CHOP, BiP/GRP78, and p-ERK 1/2, were performed (Figure 8). When A2780 cells were treated with increasing concentrations of **2** for 24 h, the dose-dependent upregulation of IRE1α and CHOP proteins, decrease of ER stress chaperone BiP/GRP78, and phosphorylation of ERK were observed as a response to ER stress. To assess the effects of **2** on the cell cycle, we examined the expression of cyclin D1 and cyclin B1 which serve as cell cycle regulatory switches in actively proliferating cells and are required for cell cycle progression in G_1 and G_2 phases, respectively. Complex **2** displayed significant inhibition of cyclin D1 expression, indicating cell cycle arrest at G_1/S phase, whereas no changes in cyclin B1 expression were detected. Subsequently, we compared the effects of **2** and the respective proligand **HL**^{2} on the expression of p-ERK1/2 and the marker of antioxidant defence NRF2. Both **HL**^{2} and **2** demonstrated phosphorylation of ERK1/2; however, the effects on NRF2 were markedly different. Whereas no increase of NRF2 expression was observed, when cells were treated with **HL**^{2}, complex **2** induced increased expression of NRF2 even at low concentration, indicating activated antioxidant defense, possibly as a result of reactive oxygen species (ROS) insult caused by Cu(II) reduction.

2.13. HL^2 and 2 Induced Dose-Dependent Apoptosis Accompanied by Poly(ADP-ribose)polymerase-1 Cleavage and XIAP Inhibition. To elucidate if observed

DOI: 10.1021/acs.jmedchem.8b01031
J. Med. Chem. 2019, 62, 512−530

cytotoxicity of new compounds described in this study was a result of apoptosis induction, we conducted Annexin V/PI apoptosis assay. In brief, fluorochrome-labeled Annexin V reagent is used for detection of membrane phosphatidylserine (PS), which translocates to the cellular surface from the inner side of plasma membrane in the event of early apoptosis. Simultaneously, PI is used for detection of later stages of apoptosis or necrosis, which are characterized by loss of membrane integrity and accumulation of PI inside the cells. A2780 cells were treated with $2IC_{50}$ and $6IC_{50}$ concentrations of $\mathbf{HL^2}$ and **2** (IC_{50} values were obtained from MTT experiment in A2780 cells with the exposure time of 72 h). Results are illustrated in Figure 9. Upon incubation of A2780 cells with increasing concentrations of $\mathbf{HL^2}$ and **2**, the dose-dependent increase of apoptotic cells was observed.

At low concentrations, both the proligand and Cu(II) complex induced a two- to three-fold increase of apoptotic cells in comparison with untreated cells [7.8 ± 1.8, 17.2 ± 3.9, and 22.5 ± 5.3% for untreated cells, $\mathbf{HL^2}$ ($2IC_{50}$) and **2** ($2IC_{50}$), respectively]. At high concentrations, a further increase of apoptotic cells was observed [28.1 ± 4.0 and 24.4 ± 7.8.% for $\mathbf{HL^2}$ ($6IC_{50}$) and **2** ($6IC_{50}$)]. No significant differences between the apoptosis-inducing properties of the proligand $\mathbf{HL^2}$ and **2** were noticed. When $CuCl_2$ was incubated with the cells at the concentration, corresponding to Cu content in **2** at $2IC_{50}$, no induction of apoptosis was detected, which can be explained by poor cellular accumulation of $CuCl_2$. The proportion of necrotic cells was negligible and no significant deviation from untreated cells was detected; therefore, the induction of necrosis by $\mathbf{HL^2}$ and **2** was ruled out. Subsequently, the effects of $\mathbf{HL^2}$ and **2** on apoptotic signaling in cells were investigated by western blotting. A2780 cells were treated with increasing concentrations of the drug for 24 h, and the cleavage of poly(ADP-ribose)polymerase-1 (PARP) was investigated (Figure 8). Cleavage of PARP through suicidal proteases such as caspases has been widely accepted as an indicator of apoptosis.[43] As can be seen in Figure 8, both $\mathbf{HL^2}$ and **2** revealed a dose-dependent PARP cleavage, indicating apoptosis induction in agreement with the results of Annexin V/PI assay. Additionally, expression of X-linked inhibitor of apoptosis (XIAP) was markedly reduced in a dose-dependent manner upon treatment with increasing concentrations of **2**.

3. DISCUSSION

The diverse biological and chemical properties of triapine and other TSCs, as well as their transition-metal complexes, have been extensively studied for decades.[41,44−51] Their antiproliferative and antibacterial activity varies greatly, from low nanomolar to high micromolar range, depending on the substituents at the TSC backbone.[16,20,52] Even though clinical trials demonstrated some benefits of patient treatment with triapine, its low aqueous solubility and high toxicity prevent it from further clinical progress. In a continuous effort to improve the bioavailability and therapeutic profile of TSCs and Cu(II)−TSC complexes, novel TSC hybrids with bioactive L-proline, homoproline, piperazine, or iminodiacetate moieties, using the molecular hybridization approach, have been designed and synthesized.[16−20] However, the improvement of the aqueous solubility was often accompanied by a significant decrease in cytotoxicity. In this study, the attachment of N-substituted morpholine moiety at the TSC backbone resulted in a simultaneous improvement of aqueous solubility and cytotoxicity (up to ∼50 times in comparison with triapine). To ensure the selectivity of novel TSCs toward cancer cells over healthy cells, their cytotoxicity against A2780 cancer cells and noncancerous HEK293 cells was compared. It was shown that new compounds were 2−5-fold more toxic toward cancer cells than healthy cells (Tables 1 and 2), whereas triapine was more toxic toward noncancerous cells, which is in agreement with its known high toxicity. The coordination of TSCs to Cu(II) resulted in Cu(II)−TSC complexes with similar or improved antiproliferative activity. In general, when TSCs are coordinated to Cu(II), an increase in cytotoxicity is observed;[17,18,53] however, Cu(II)−triapine complex was shown to be significantly less cytotoxic than triapine itself.[27] The activity of the Cu(II) complexes **1**−**6** was in a good correlation with their lipophilicity, cellular accumulation, and their electrochemical redox potentials (Tables S6 and 2). Interestingly, metal-free TSCs exhibited only low antibacterial properties against *S. aureus*, whereas Cu(II)−TSC complexes revealed significant antibacterial activity similar to that of the commonly used antibiotic CPX (Table 3). These results indicate that coordination of TSCs to Cu(II) improved their therapeutic potential. It should be noted that the replacement of N,N,S- with N,N,N-chelating moiety in **6** resulted in a drop of cytotoxicity and antibacterial activity, which is in agreement with the previously reported data.[20]

The antiproliferative activity of triapine and other TSC proligands is often related to their Fe-chelating properties.[54] To sustain their high proliferation rate, cancer cells rely on increased uptake of Fe from Fe-transporting proteins; therefore, Fe chelation is a valuable therapeutic strategy for cancer treatment. On the basis of UV−vis and ESI-MS experiments, it was demonstrated that irrespective of metal-to-ligand ratio, proligands $\mathbf{HL^2}$ and $\mathbf{HL^5}$ readily reacted with Fe(III) to form $[Fe^{III}(L^2)_2]^+$ and $[Fe^{III}(L^5)_2]^+$ species, which could be reduced to Fe(II) bis-ligand complexes by the reducing agent DTT. These results indicate that morpholine−TSC hybrids, investigated in this study, may act as Fe chelators. Additionally, spectroelectrochemical experiments revealed that under reducing conditions, the Cu(II)−TSC complexes could undergo reversible reduction to Cu(I) species, with simultaneous release of proligands, suggesting that these complexes may act as Fe chelators, also in cancer cells. In addition, the presence of the Cu(II) ion in the cells may lead to the production of ROS in vivo because of Cu(II)/Cu(I) redox cycling.[55]

It is well known that one of the mechanisms contributing to the cytotoxic effects of Fe chelators is inhibition of the RNR enzyme, which is highly expressed in cancer cells, and essential for their DNA synthesis. The mechanism of RNR inhibition by triapine has been extensively studied by several research groups.[41,46,47,51,56] It has been proposed that triapine interferes with the assembly of the differic-tyrosyl radical cofactor in R2, necessary for the catalytic activity of RNR.[46,56] Moreover, it has been shown that the presence of Fe is required for effective R2 inhibition,[44,45] and that it is actually the Fe(II)−triapine species that is responsible for the R2-specific RNR inhibitory effect of triapine.[41,46,47,51,58] The Fe(II)−triapine complex may be formed by chelation of Fe from the differic cofactor in R2 in vitro[41,44] and/or from intracellular iron pools in vivo.[46,56] The potent inhibition of human[47] and mouse[41] R2 RNR in vitro by catalytic amounts of Fe(II)−triapine has been proposed to involve ROS. Namely, ROS had been spin-trapped and

DOI: 10.1021/acs.jmedchem.8b01031
J. Med. Chem. 2019, 62, 512−530

detected by EPR spectroscopy, in the aerobic reaction between human R2 RNR and Fe(II)−triapine, which had implicated that O_2 is important in tyrosyl radical destruction and that ROS may ultimately be responsible for the pharmacologic effects of triapine in vivo.[47] In another study of time-dependent tyrosyl radical reduction in mouse R2 by triapine and its Zn, Ga, Cu, and Fe complexes, the requirement of O_2 in R2 inhibition was also suggested.[41] This was based on the observation that substoichiometric amounts of Fe(III)−triapine relative to R2 (protein-to-complex mole ratio, 5:1) reduced only 20% tyrosyl radical in anaerobic conditions, compared with 100% in aerobic conditions. However, more recently, in a different experimental setup, namely, in the presence of a 10-fold excess of Fe(II)−triapine over R2 protein, the role of ROS (and O_2) in human R2 inhibition was excluded.[51] This study showed that the principle mechanism of human R2 RNR inhibition by triapine, based on kinetic measurements of tyrosyl radical, and ^{55}Fe loss, is direct radical quenching, in an iron-loaded protein. Furthermore, it implied that Fe(II)−triapine can rapidly reduce the tyrosyl radical, while leaving the protein in the met-state.

To investigate if R2 RNR could be the potential biomolecular target for the novel morpholine−TSC hybrids, as well as their Cu(II) complexes, molecular docking studies, as well as R2 RNR tyrosyl radical reduction kinetic experiments, were performed. It has been suggested that the efficiency of R2 inhibition is likely to depend on the access of the inhibitors to the differic center of R2;[41,47] therefore, we estimated the likelihood of the binding of TSC proligands **HL^1**−**HL^6** and their corresponding Cu(II) complexes **1**−**6** to the surface of the R2 protein. It was demonstrated that new TSCs and their Cu(II) complexes were deeply embedded into the pocket of the R2 protein and exhibited hydrogen bonding patterns similar to triapine (Figure 7). On the basis of the results of the molecular docking studies suggesting plausible binding to the mouse R2 protein, the time-dependent tyrosyl radical reduction in the mouse R2 protein upon incubation with the most cytotoxic complexes, **2** and **5**, and the corresponding proligands **HL^2** and **HL^5**, at a 1:1 protein-to-compound ratio, was measured by EPR spectroscopy. Only in the presence of DTT (which can reduce Fe(III) to Fe(II) in the R2 differic cofactor),[40] **HL^2** and **HL^5** caused 50% tyrosyl radical reduction (Figure S15a). These results show that R2 inactivation by **HL^2** and **HL^5** is not as efficient as with triapine, which causes 100% tyrosyl radical loss in mouse R2 after 5 min (in the same experimental conditions).[41] The most plausible explanation for this observation is that different mechanisms are likely to be involved in R2 inhibition by **HL^2**, **HL^5**, and triapine. The R2 inhibitory activity of the corresponding Cu(II) complexes **2** and **5** was found to be similar to that of the proligands (Figure S15a). This is likely due to the fact that in the presence of DTT, the reduction of Cu(II) to Cu(I) leads to the release of the proligands, which is in agreement with the results of spectroelectrochemical experiments (vide supra). Because the UV−vis, and ESI-MS experiments showed that **HL^2** and **HL^5** act as tridentate ligands, and form stable Fe(II)L_2 complexes (Figure S15c,d and S16), it is possible to propose that the mechanism of R2 inhibition by the TSC proligands involves Fe chelation from the differic cofactor. On the basis of the extent of tyrosyl radical reduction, it is tempting to speculate that the subsequently formed Fe(II) complexes are not potent inhibitors like the Fe(II)−triapine complex. However, as this was not the aim of this paper, it is reasonable to refrain from any conclusions prior to the detailed mechanistic studies of mouse, human, and p53 R2 RNR inhibition by the morpholine−TSC hybrids. Moreover, a separate study should be dedicated only to the comparison of the inhibitory potentials of selected TSCs, as well as their Fe(II) complexes, to comprehensively understand the structure−activity relationships, which in turn may explain the mechanism of R2 RNR inhibition. Finally, even though R2 inhibition can be partially attributed to the marked anticancer activity of **2** and **5**, other biomolecular targets are likely to be involved (Figure 10).

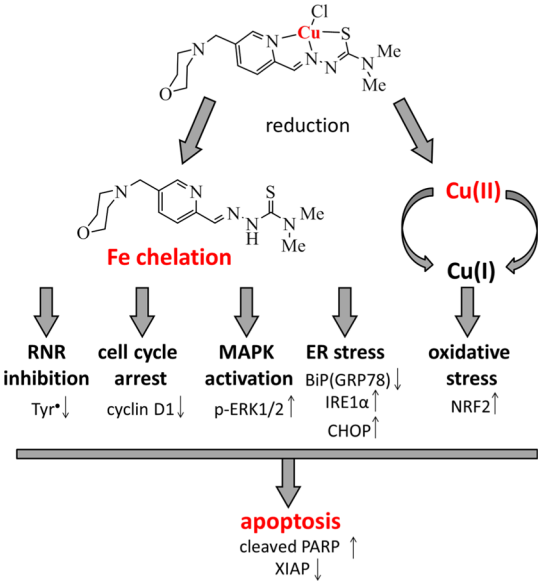

Figure 10. Proposed molecular mechanism of cytotoxicity of **2**.

Fe homeostasis is an intrinsically complex process; hence, Fe sequestration results in the alteration of various biomolecular pathways. Besides RNR, Fe depletion affects multiple molecular targets including those regulating the cell cycle.[57] It has been reported that the expression of cyclin D1, which ensures the progression through the G_1/S phase, was strongly dependent on the cellular Fe status.[58] It is believed that in Fe-depleted conditions, down-regulation of cyclin D1 prevents cells from entering the S phase, where Fe is needed for the activity of the RNR enzyme and DNA synthesis.[59] Fe chelation by TSCs often results in the down-regulation of cyclin D1 and subsequent cell cycle arrest at the G_1/S phase.[60,61] As expected, complex **2** was shown to induce strong dose-dependent down-regulation of cyclin D1, whereas the protein expression of cyclin B1, which is responsible for G_2/M progression, remained unchanged. To further investigate the potential biomolecular targets of Fe-chelating compounds of interest, we studied the phosphorylation of ERK protein, which belongs to the MAPK family. The MAP kinases occupy the central position in cell growth and apoptosis, and each MAP kinase member plays a different role in cellular responses.[62] It was reported that some Fe chelators induced cancer cell death associated with the activation of p38 MAPK and ERK.[63] Moreover, the MAPK-mediated cell death was characterized by the decreased expression of cyclin D1.[64] Complex **2**, as well as the corresponding proligand **HL^2**, caused dose-dependent phosphorylation of ERK in line with its activation, suggesting

DOI: 10.1021/acs.jmedchem.8b01031
J. Med. Chem. 2019, 62, 512−530

that MAPK pathway might be a potential mediator of the cell death, induced by this complex.

Recently, it was discovered that chelation and depletion of intracellular Fe leads to the activation of certain ER stress-response proteins.[65,66] Previously, several TSCs and their Cu(II) complexes were reported to induce ER stress, characterized by unfolded protein response (UPR) activation,[67,68] ER expansion, and release of intracellular calcium.[69] Because under reducing conditions, the TSCs and their Cu(II) complexes demonstrated formation of Fe(II)−TSC complexes, it may be suggested that they could possibly induce sequestration of cellular Fe resulting in the ER stress. It occurs due to the accumulation of misfolded and/or unfolded proteins in ER, resulting in the disruption of cellular homeostasis. To overcome stress, cells activate a rescue program known as UPR, which operates via several signaling pathways, namely, ATF6, PERK, and IRE1α. However, in case of severe ER stress, the pro-survival program is switched off and pro-apoptotic signaling takes place, characterized by the enhanced expression of CHOP protein. Complex **2** was shown to induce dose-dependent increase in the expression of IRE1α and CHOP proteins, indicating the induction of UPR signaling as a result of ER stress. Cell treatment with **2** resulted in a concentration-dependent decrease of BiP/GRP78 protein marker. The ER chaperon BiP/GRP78 plays a central role in the survival machinery and its overexpression is associated with tumor progression and metastases.[70] The inhibition of BiP/GRP78 indicates severe ER stress, resulting in the suppression of pro-survival chaperones. The antibacterial properties of novel Cu(II)−TSC complexes can be also related to ER stress induction because it was recently demonstrated in in vitro and in vivo experiments that chemical modulation of ER stress might result in the overload of its machinery that can be effective in elimination of bacterial infection.[71] Additionally, it was reported that efficient killing of methicillin-resistant *S. aureus* was dependent on the induction of IRE1α UPR pathway and required sustained generation of ROS.[72] On the basis of the observations that **2**, but not proligand $\mathbf{HL^2}$, induced antioxidant defence in cancer cells characterized by NRF2 induction, it may be speculated that the ability of **2**, but not proligand $\mathbf{HL^2}$, to induce oxidative and ER stress, may be related to the beneficial antibacterial activity of Cu(II)−TSC complexes over metal-free TSCs. However, it is not clear yet why new complexes **1**−**6** did not inhibit the growth of *P. aeruginosa* and their mechanism of action should be investigated in more detail.

To cope with the severe perturbations imposed by drug treatment, cancer cells develop adaptive responses to provide them with survival advantage. However, TSCs and their Cu(II) complexes significantly disturbed cellular life-death balance toward cell death, resulting in the induction of apoptosis. Both proligand $\mathbf{HL^2}$ and complex **2** were demonstrated to induce apoptosis characterized by PARP cleavage, decreased expression of XIAP, and increased PS translocation. It should be noted that XIAP is a determining factor of cisplatin chemoresistance in ovarian cancer cells, as it effectively suppresses apoptosis via caspase-3 and caspase-7 inhibition.[73] Therefore, the ability of **2** to decrease XIAP expression is highly important and to the best of our knowledge has not been previously reported for TSCs and metal thiosemicarbazonates, with the exception of triapine.[74] Some TSCs and their respective Cu(II) complexes have been reported to simultaneously induce various types of cell death including apoptosis,[75,76] autophagy[63,77] and methuosis, which is a very special form of nonapoptotic cell death involving massive cytoplasmic vacuolization.[78] Therefore, induction of other forms of cell death by new TSCs and their Cu(II) complexes presented in this study cannot be excluded. The results show that the attachment of the morpholine moiety at the TSC backbone and the subsequent coordination to Cu(II) resulted in new drug candidates, likely with better therapeutic profile than triapine and a promising potential for further clinical development.

4. CONCLUSIONS

One of the reasons hindering the clinical development of Cu(II) TSC complexes is their low aqueous solubility. The decoration of the TSC backbone with functional groups that increase the aqueous solubility and bioavailability often results in a significant decrease of the compound activity. In this work, attachment of a morpholine moiety to 2-formylpyridine (iso)TSC in position 5 of 2-formylpyridine moiety yielded new water-soluble TSC−morpholine hybrids and their Cu(II) complexes, which demonstrated high antiproliferative activity against cisplatin-sensitive and cisplatin-resistant ovarian carcinoma cells, in a nanomolar to submicromolar concentration range. Sufficient aqueous solubility of the new compounds enabled the study of their solution behavior and electrochemical properties under conditions similar to the intracellular environment. Solution speciation studies of **1** revealed that the dissociation of the complex does not occur at the physiological pH, even at micromolar concentrations, indicating its high stability in aqueous media. However, under reducing conditions associated with the cancer cell environment, the reversible reduction of Cu(II) with subsequent release of the proligand within the biologically accessible electrochemical window is plausible. Because the R2 RNR protein is believed to be one of the biomolecular targets of TSCs, and the fact that the proligands form 2:1 complexes with Fe(II), the chelation of Fe(II) from R2 was expected. The Cu(II)−TSCs and their corresponding proligands showed only moderate tyrosyl radical reduction in mouse R2. Therefore, the marked anticancer activity of the compounds investigated in this work was not solely related to their RNR inhibitory potential but also to the induction of apoptosis as a result of ER stress, MAPK activation, and cell cycle perturbations. Studies of the mechanisms controlling cellular accumulation of the lead drug **2** have shown that it accumulates in cancer cells as a result of passive and/or facilitated diffusion. Finally, it was discovered that coordination of TSC ligands to Cu(II) resulted in a significant enhancement of their antibacterial properties against *S. aureus*. The combination of excellent antiproliferative and antibacterial activity, as well as water-solubility, is a sound basis for further development of this class of Cu(II) thiosemicarbazonates as dual pharmaceutical agents.

5. EXPERIMENTAL SECTION

5.1. Chemicals. 2,5-Pyridinecarboxylic acid was received from Alfa Aesar. EDTA, KOH, and 4-(2-hydroxyethyl)-1-piperazineethanesulfonic acid (HEPES) were purchased from Sigma-Aldrich in puriss quality. KCl, $CuCl_2$, hydrochloric acid, and *n*-octanol are products of Molar Chemicals. $CuCl_2$ stock solution was prepared from anhydrous $CuCl_2$ and water, and its exact concentration was determined by complexometry through the EDTA complex. All solvents were of analytical grade and used without further purification. Milli-Q water was used for sample preparation. The synthesis of the 5-

DOI: 10.1021/acs.jmedchem.8b01031
J. Med. Chem. 2019, 62, 512−530

methylmorpholine-pyridine-2-carboxaldehyde **H** (Scheme 1) is described in detail in the Supporting Information. Chemical grade cisplatin (1 mg/mL) was purchased from Hospira Pty Ltd (Melbourne, Australia). IGEPAL CA-630, DL-dithiothreitol (DTT), tetramethylethylenediamine, sodium deoxycholate, nonfat dried milk bovine, TWEEN 20, ponceau S, and PI were purchased from Sigma-Aldrich (St Louis, MO, USA). Thiazolyl blue tetrazolium bromide (MTT) was purchased from Alfa Aesar, while Tris was purchased from Vivantis Technologies. Glycine, Hyclone Trypsin Protease 2.5% (10×) solution, RPMI 1640, Dulbecco's modified Eagle's medium (DMEM) medium, fetal bovine serum (FBS), bovine serum albumin (BSA), HBSS and Pierce Protease, and Phosphatase Inhibitor Mini Tablets were from Thermo Fisher Scientific. Hyclone Dulbecco's phosphate-buffered saline (10×) was received from GE Healthcare Life Sciences. Biorad protein assay dye reagent concentrate, 30% acrylamide/bis solution, 5× Laemmli sample buffer, and nitrocellulose membrane (0.2 μm) were from Bio-Rad Laboratories. Luminata Classico and Crescendo Western HRP substrate were purchased from Merck Millipore Corporation. Milli-Q-grade purified water was obtained from a Milli-Q UV purification system (Sartorius Stedim Biotech S.A., Aubagne Cedex, France). All antibodies were from Cell Signaling Technologies (Beverly, MA, USA). Nitric acid (65 to 71%, *Trace*SELECT Ultra) for ICP−MS analysis and nBu$_4$NPF$_6$ for cyclic voltammetry experiments were obtained from Fluka (Sigma Aldrich) and used without further purification. Cu and In standards for ICP−MS measurements were obtained from CPI international (Amsterdam, The Netherlands). Cycloheximide, oligomycin, and annexin V-FITC apoptosis detection reagent (500×) were purchased from Abcam (Cambridge, UK).

5.2. Synthesis of Proligands. The yields, mp, and analytical data for **HL^1**−**HL^6** and **1**−**6** are presented in Tables S9 and S10. The experimental CHNS contents were within ±0.4 with those calculated, providing evidence for ≥95% purity.

*5.2.1. 5-(Morpholinomethyl)pyridine-2-carboxaldehyde Thiosemicarbazone (**HL^1**).* 5-Morpholinomethyl-pyridine-2-carboxaldehyde (0.29 g, 1.41 mmol), thiosemicarbazide (0.13 g, 1.41 mmol), and EtOH (5 mL) were mixed in a 25 mL Schlenk tube. The reaction mixture was stirred at 78 °C overnight. The next day, the reaction mixture was cooled to room temperature and stored at 4 °C for 4 h. The white crystalline precipitate was filtered off, washed with cold EtOH, and dried in vacuo. Yield: 0.34 g. ^{1}H NMR 500 MHz (DMSO-d_6, δ, ppm): ^{1}H NMR (500 MHz, DMSO): δ 11.62 (s, 1H, NH^{16}), 8.48 (d, J = 1.3 Hz, 1H, H^5), 8.34 (s, 1H, NH^{19}), 8.24 (d, J = 8.1 Hz, 1H, H^2), 8.15 (s, 1H, NH^{19}), 8.09 (s, 1H, H^{14}), 7.74 (dd, J = 8.2, 1.7 Hz, 1H, H^4), 3.59−3.54 (m, 4H, H^{10}, H^{12}), 3.51 (s, 2H, H^7), 2.36 (s, 4H, H^9, H^{13}). ^{13}C NMR (126 MHz, DMSO): δ 178.74 (C$_q$, C^{17}), 152.73 (C$_q$, C^2), 150.12 (CH, C^6), 142.85 (CH, C^{14}), 137.51 (CH, C^4), 134.23 (C$_q$, C^5), 120.23 (CH, C^3), 66.57 (2CH$_2$, C^{10}, C^{12}), 59.74 (CH$_2$, C^7), 53.49 (2CH$_2$, C^9, C^{13}). IR (ATR, selected bands, $\tilde{\nu}_{max}$): 1612, 1527, 1468, 1400, 1339, 1274, 1102, 1004, 938, 859, 626 cm^{-1}.

*5.2.2. 5-(Morpholinomethyl)pyridine-2-carboxaldehyde 4,4-Dimethyl-3-thiosemicarbazone (**HL^2**).* 5-(Morpholinomethyl)pyridine-2-carboxaldehyde (0.29 g, 1.41 mmol) and 4,4-dimethyl-3-thiosemicarbazide (0.17 g, 1.41 mmol) were dissolved in EtOH (5 mL) and stirred in a Schlenk tube at 78 °C for 2 h until the solution became clear. The reaction mixture was left to stand at 4 °C for 6 h. The yellow crystalline precipitate was filtered off, washed with cold EtOH, and dried in vacuo. Yield: 0.25 g. ^{1}H NMR (500 MHz, DMSO): δ 15.08 (s, 1H, NH^{16}), 8.71 (s, 1H, H^3), 8.49 (s, 1H, H^6), 8.23 (d, 1H, H^{14}), 7.76 (dd, J = 13.9, 8.1 Hz, 1H, H^4), 3.59 (s, 4H, H^{10}, H^{12}), 3.52 (s, 2H, H^7), 3.38 (s, 4H, H^{20}, H^{21}), 2.37 (s, 4H, H^9, H^{13}).·^{13}C NMR (126 MHz, DMSO): δ 180.02 (C$_q$, C^{17}), 153.06 (C$_q$, C^2), 150.27 (CH, C^6), 148.84 (CH, C^3), 144.29 (CH, C^{14}), 137.75 (CH, C^4), 134.06 (C$_q$, C^5), 66.61 (2CH$_2$, C^{10}, C^{12}), 59.77 (CH$_2$, C^7), 53.53 (2CH$_2$, C^9, C^{13}), 42.72 (2CH$_3$, C^{20}, C^{21}). IR (ATR, selected bands, $\tilde{\nu}_{max}$): 1497, 1443, 1362, 1303, 1209, 1158, 1108, 1064, 1003, 901, 862, 716, 627 cm^{-1}.

*5.2.3. 5-(Morpholinomethyl)pyridine-2-Carboxaldehyde N-Pyrrolidinylthiosemicarbazone (**HL^3**).* 5-(Morpholinomethyl)pyridine-2-carboxaldehyde (0.29 g, 1.41 mmol) and *N*-pyrrolidine-3-thiosemicarbazide (0.20 g, 1.41 mmol) were dissolved in EtOH (5 mL) and stirred in a Schlenk tube at 78 °C for 2 h until the solution became clear. The mixture was left to stand at 4 °C for 12 h. The yellow crystalline precipitate was filtered off, washed with cold EtOH, and dried in vacuo. Yield: 0.36 g. ^{1}H NMR (500 MHz, DMSO): δ 11.23 (s, 1H, NH^{16}), 8.49 (d, J = 1.4 Hz, 1H, H^3), 8.20 (s, 1H, H^6), 8.01 (dd, J = 8.0, 2.1 Hz, 4H, H^{21}, H^{22}), 7.84 (s, 1H, H^{14}), 7.77 (d, J = 1.9 Hz, 1H, H^4), 3.76 (s, 4H, H^{20}, H^{23}), 3.59 (dd, J = 8.1, 5.3 Hz, 4H, H^9, H^{13}), 3.52 (s, 2H, H^7), 2.42−2.32 (m, 4H, H^{10}, H^{12}). ^{13}C NMR (126 MHz, DMSO): δ 177.02 (C$_q$, C^{17}), 153.11 (C$_q$, C^2), 150.17 (CH, C^6), 149.02 (CH, C^3), 143.48 (CH, C^{14}), 139.44, (2CH$_2$, C^{21}, C^{22}), 138.08 (CH, C^{16}), 134.05 (C$_q$, C^5), 119.43 (CH, C^3), 66.62 (2CH$_2$, C^9, C^{13}), 59.91 (CH$_2$, C^7), 53.53 (2CH$_2$, C^{20}, C^{23}), 40.00 (2CH$_2$, C^{10}, C^{12}, overlapped with residual DMSO signal). IR (ATR, selected bands, $\tilde{\nu}_{max}$): 1585, 1529, 1419, 1347, 1287, 1108, 1001, 855, 796, 741 cm^{-1}.

*5.2.4. 5-(Morpholinomethyl)pyridine-2-carboxaldehyde N-Morpholinylthiosemicarbazone (**HL^4**).* 5-(Morpholinomethyl)pyridine-2-carboxaldehyde (0.29 g, 1.41 mmol) and *N*-morpholinyl-3-thiosemicarbazide (0.23 g, 1.41 mmol) were dissolved in EtOH (5 mL) and stirred in a Shlenk tube at 78 °C for 2.5 h until the solution became clear. Light-yellow crystals formed within 3 weeks at 4 °C after concentration of the reaction mixture. These were filtered off, washed with cold EtOH, and dried in vacuo. Yield: 0.12 g. ^{1}H NMR (500 MHz, DMSO): δ 11.43 (s, 1H, NH^{16}), 8.50 (d, J = 1.3 Hz, 1H, H^6), 8.18 (s, 1H, H^{14}), 7.83 (d, J = 8.1 Hz, 1H, H^4), 7.78 (dd, J = 8.2, 1.9 Hz, 1H, H^3), 3.98−3.91 (m, 4H, H^{20}, H^{24}), 3.72−3.66 (m, 4H, H^{21}, H^{23}), 3.60−3.55 (m, 4H, H^9, H^{13}), 3.52 (s, 2H, H^7), 2.36 (br s, 4H, H^{10}, H^{12}). ^{13}C NMR (126 MHz, DMSO): δ 181.27 (C$_q$, C^{17}), 152.75 (C$_q$, C^4), 150.33 (CH, C^6), 144.44 (CH, C^{14}), 137.83 (CH, C^3), 134.27 (CH, C^2), 119.60 (C$_q$, C^4), 66.60 (2CH$_2$, C^{21}, C^{23}), 66.48 (CH$_2$, C^7), 59.73 (2CH$_2$, C^9, C^{13}).

*5.2.5. 5-(Morpholinomethyl)pyridine-2-carboxaldehyde 4-Phenylthiosemicarbazone (**HL^5**).* 5-(Morpholinomethyl)pyridine-2-carboxaldehyde (0.29 g, 1.41 mmol) and 4-phenyl-3-thiosemicarbazide (0.24 g, 1.41 mmol) were dissolved in EtOH (5 mL) and stirred in a Schlenk tube at 78 °C for 3 h until the solution became clear. Then, the reaction mixture was allowed to stand at 4 °C for 12 h. The yellow crystalline precipitate was filtered off, washed with cold EtOH, and dried in vacuo. Yield: 0.32 g. ^{1}H NMR (500 MHz, DMSO): δ 12.02 (s, 1H, NH^{16}), 10.24 (s, 1H, NH^{18}), 8.52 (s, 1H, H^6), 8.41 (d, J = 8.1 Hz, 1H, H^3), 8.21 (s, 1H, H^{14}), 7.78 (d, J = 10.1 Hz, 1H, H^4), 7.56 (d, J = 8.6 Hz, 2H, H^{21}, H^{25}), 7.40 (t, J = 7.9 Hz, 2H, H^{22}, H^{24}), 7.24 (t, J = 7.4 Hz, 1H, H^{23}), 3.59 (s, 4H, H^{10}, H^{12}), 3.54 (s, 2H, H^7), 2.38 (s, 4H, H^9, H^{13})·^{13}C NMR (126 MHz, DMSO) δ 176.84 (C$_q$, C^{17}), 152.62 (C$_q$, C^2), 150.25 (CH, C^6), 143.45 (C$_q$, C^{14}), 139.44 (C$_q$, C^{20}), 137.51 (CH, C^4), 134.46 (C$_q$, C^5), 128.59 (2CH, C^{22}, C^{24}), 126.56 (2CH, C^{21}, C^{25}), 120.68 (CH, C^3), 66.62 (2CH$_2$, C^{10}, C^{12}), 53.54 (2CH$_2$, C^9, C^{13}), 40.00 (CH$_2$, C^7). IR (ATR, selected bands, $\tilde{\nu}_{max}$): 1592, 1505, 1466, 1338, 1291, 1188, 1105, 1060, 1000, 944, 909, 863, 791, 751, 689, 634 cm^{-1}.

*5.2.6. 5-(Morpholinomethyl)pyridine-2-carboxaldehyde S-Methylisothiosemicarbazone (**HL^6**).* To a solution of 5-(morpholinomethyl)pyridine-2-carboxaldehyde (0.29 g, 1.41 mmol) in EtOH (6 mL) was added a solution of *S*-methylisothiosemicarbazide hydroiodide (0.33 g, 1.41 mmol) in water (2 mL). Then, the reaction mixture was heated to 60 °C and a solution of NaHCO$_3$ (0.118 g, 1.41 mmol) in water (4 mL) was added dropwise. When bubbles of CO$_2$ disappeared, the mixture was allowed to cool to room temperature. The solvent was removed under reduced pressure and the residue dissolved in water. The product was extracted with chloroform. After removal of the solvent, the residue was dissolved in a small amount of EtOH and allowed to stand at −20 °C overnight. Light-brown crystalline product was obtained the next day. Yield: 0.14 g. ^{1}H NMR (500 MHz, DMSO): δ 8.49 (d, J = 1.4 Hz, 1H, H^4), 8.21 (d, J = 8.1 Hz, 1H, H^{14}), 8.17 (s, 1H, H^6), 7.84 (d, J = 8.1 Hz, 1H, H^3), 7.16 (s, 2H, H^{18}), 3.60−3.55 (m, 8H, H^9, H^{13}), 3.51 (s, 2H, H^7), 2.40 (br s, 3H, H^{20}), 2.36 (d, J = 6.0 Hz, 8H, H^{10}, H^{12}). ^{13}C NMR (126 MHz, DMSO) δ 164.19 (C$_q$, C^{17}), 154.02 (C$_q$, C^5), 151.84 (CH, C^6), 150.12 (CH, C^4), 137.35 (CH, C^3), 133.89, (C, C^2),

DOI: 10.1021/acs.jmedchem.8b01031
J. Med. Chem. 2019, 62, 512−530

120.68 (CH, C^{14}), 66.61 ($2CH_2$, C^9, C^{13}), 59.84 (CH_2, C^7), 53.53 ($2CH_2$, C^{10}, C^{12}), 12.52 (CH_3, C^{20}). IR (ATR, selected bands, $\tilde{\nu}_{max}$): 1600, 1497, 1472, 1335, 1290, 1111, 1069, 1015, 931, 870, 790, 752, 714, 626 cm^{-1}.

5.3. Synthesis of Cu(II) Complexes. *5.3.1. [Cu(L¹)Cl] (1).* To **HL¹** (100 mg, 0.36 mmol) in MeOH (20 mL) was added triethylamine (50 μL, 0.36 mmol) and then $CuCl_2·2H_2O$ (60 mg, 0.36 mmol) in MeOH (5 mL) at 60 °C. The solution was stirred for 5 min and left to stand at room temperature overnight. The precipitate formed was filtered off, washed with cold EtOH, and dried in air. Yield: 123 mg. IR (ATR, selected bands, $\tilde{\nu}_{max}$): 1631, 1426, 1310, 1158, 1107, 1060, 907, 722, 688 cm^{-1}.

5.3.2. [Cu(L²)Cl] (2). To **HL²** (100 mg, 0.32 mmol) in MeOH (20 mL) was added triethylamine (44.5 μL, 0.32 mmol) and then $CuCl_2·2H_2O$ (54 mg, 0.32 mmol) in MeOH (5 mL) at 60 °C. The solution was stirred for 5 min and left to stand at room temperature overnight. The precipitate formed was filtered off, washed with cold EtOH, and dried in air. Yield: 104 mg. IR (ATR, selected bands, $\tilde{\nu}_{max}$): 1505, 1372, 1310, 1252, 1111, 1000, 913, 872, 749, 626 cm^{-1}.

5.3.3. [Cu(L³)Cl] (3). To **HL³** (100 mg, 0.3 mmol) in MeOH (20 mL) was added triethylamine (42 μL, 0.28 mmol) and then $CuCl_2·2H_2O$ (50 mg, 0.3 mmol) in MeOH (5 mL) at 60 °C. The solution was stirred for 5 min and left to stand at room temperature overnight. The precipitate formed was filtered off, washed with cold EtOH, and dried in air. Yield: 74 mg. IR (ATR, selected bands, $\tilde{\nu}_{max}$): 1444, 1375, 1281, 1242, 1111, 1004, 913, 885, 623 cm^{-1}.

5.3.4. [Cu(L⁴)Cl] (4). To **HL⁴** (50 mg, 0.28 mmol) in MeOH (20 mL) was added triethylamine (20 μL, 0.28 mmol) and then $CuCl_2·2H_2O$ (25 mg, 0.28 mmol) in MeOH (5 mL) at 60 °C. The solution was stirred for 5 min and left to stand at room temperature overnight. The precipitate formed was filtered off, washed with cold EtOH, and dried in air. Yield: 22 mg. IR (ATR, selected bands, $\tilde{\nu}_{max}$): 1465, 1429, 1381, 1313, 1265, 1229, 1109, 1028, 932, 888, 860 cm^{-1}.

5.3.5. [Cu(L⁵)Cl] (5). To **HL⁵** (100 mg, 0.28 mmol) in MeOH (20 mL) was added triethylamine (39 μL, 0.28 mmol) and then $CuCl_2·2H_2O$ (47 mg, 0.82 mmol) in MeOH (5 mL) on heating. The solution was stirred for 5 min and left to stand at room temperature overnight. The precipitate formed was filtered off, washed with cold EtOH, and dried in air. Yield: 67 mg. IR (ATR, selected bands, $\tilde{\nu}_{max}$): 1600, 1550, 1493, 1417, 1182, 1111, 1000, 899, 863, 799, 752, 691 cm^{-1}.

5.3.6. [Cu(L⁶)Cl] (6). To **HL⁶** (100 mg, 0.34 mmol) in MeOH (20 mL) was added triethylamine (47 μL, 0.34 mmol). Then, the reaction was heated to 40 °C and $CuCl_2·2H_2O$ (58 mg, 0.34 mmol) in MeOH (5 mL) was added. The solution was stirred for 5 min at 50 °C and left to stand at −20 °C overnight. The precipitate formed was filtered off, washed with ethanol, ether, and dried in air. Yield: 75 mg. IR (ATR, selected bands, $\tilde{\nu}_{max}$): 1599, 1491, 1431, 1320, 1115, 1035, 1004, 973, 911, 796, 724 cm^{-1}.

5.4. Solution Equilibrium Studies in Aqueous Phase. *5.4.1. pH-Potentiometric Measurements.* These measurements were performed as described previously.[16] The initial volume of the samples was 10.0 mL. The proligand concentration was 1 mM and metal ion-to-ligand ratios of 1:1 to 1:3 were used. The exact concentration of the proligand stock solutions together with the proton dissociation constants were determined by pH-potentiometric titrations with the use of the computer program HYPERQUAD.[79] HYPERQUAD was also utilized to establish the stoichiometry of the complexes and to calculate the stability constants ($\log \beta(M_pL_qH_r)$). $\beta(M_pL_qH_r)$ is defined for the general equilibrium $pM + qL + rH \rightleftharpoons M_pL_qH_r$ as $\beta(M_pL_qH_r) = [M_pL_qH_r]/[M]^p[L]^q[H]^r$, where M denotes the metal ion and L denotes the completely deprotonated ligand. The uncertainties (SDs) of the equilibrium constants are shown in parentheses for the species determined in the present work.

5.5. Instrumentation. ICP−Optical Emission Spectroscopy (OES) determination of the Cu content was performed in Chemical, Molecular and Analysis Centre, National University of Singapore with Optima ICP−OES (PerkinElmer, Watham, MA, USA). The absorbance of thiazolyl blue tetrazolium bromide (MTT) was measured by synergy H1 hybrid multimode microplate reader (Bio-Tek, Winoosky, VT, USA). Cu and Re contents in cells were determined by Agilent 7700 Series ICP−MS (Agilent Technologies, Santa Clara, CA, USA). Flow cytometry was performed on BD LSRFortessa Cell Analyzer (BD Biosciences, Franklin Lakes, NJ, USA). Western blot images were generated from G:Box (Syngene, Cambride, UK). The UV−vis spectrophotometric measurements were performed on a Hewlett Packard 8452A diode array spectrophotometer and a Thermo Scientific Evolution 220 spectrophotometer. CW-EPR spectra were recorded with a BRUKER EleXsys E500 spectrometer. In situ ultraviolet−visible−near-infrared (UV−vis−NIR) spectroelectrochemical measurements were performed on a spectrometer (Avantes, Model AvaSpec-2048x14-USB2.

5.6. UV−Vis Spectrophotometric, ^{1}H NMR, EPR, and Lipophilicity Measurements. UV−vis spectra were recorded in the ranges 200−800 and 450−1050 nm, respectively. The path length was 0.5, 1, or 2 cm. Stability constants of the complexes and the molar absorbance spectra of the individual species were calculated with the computer program PSEQUAD.[80] The spectrophotometric titrations were performed on samples containing the proligand with or without Cu(II) ions and the concentration of the proligand was 120 μM to 1.4 mM. The metal-to-proligand ratios were 1:1 and 1:2 in the pH range from 1.0 to 11.5 at 25.0 ± 0.1 °C at an ionic strength of 0.10 M (KCl). pH values in the range 1.0−2.0 were calculated from the strong acid and strong base content. The conditional stability constant of [CuL] at pH 6.0 (50 mM MES) for **1** was determined from competition titrations of the Cu(II) complex of EDTA with the proligand **HL¹**. Samples contained 34 μM Cu(II) ion and 34 μM **HL¹**, and the concentration of the EDTA was varied in the range of 0−83 μM. Absorbance data were recorded after 0.5 h incubation. ^{1}H NMR studies for **HL¹** were carried out on a Bruker Avance III HD Ascend 500 Plus instrument in a 10% (v/v) D_2O/H_2O mixture at ionic strength of 0.10 M (KCl). All CW-EPR spectra were recorded with a BRUKER EleXsys E500 spectrometer (microwave frequency 9.85 GHz, microwave power 10 mW, modulation amplitude 5 G, modulation frequency 100 kHz). The pH-dependent series of isotropic EPR spectra were recorded in a circulating system, at room temperature. A Heidolph Pumpdrive 5101 peristaltic pump was used for circulating the solution from the titration pot through a capillary tube into a Bruker flat cell placed in the cavity of the instrument. The titrations were carried out under a nitrogen atmosphere. EPR spectra were recorded at 1.00 mM Cu(II) and 0.75 mM ligand concentration, and at 1.00 mM $CuCl_2$ and 1.50 mM ligand concentration, both between pH 1 and 11.5. The ionic strength of 0.1 M was adjusted with KCl. Before the simulation of the room temperature spectra, the measured spectra were corrected by subtracting the spectra of aqua solution measured in the same circulating system. The series of pH-dependent isotropic EPR spectra recorded in the equimolar solution were simulated by the "two-dimensional" method using the 2D_EPR program[81] and EPR parameters were computed as published previously.[16,25] Distribution coefficients ($D_{7.4}$) values of complexes **1**−**6** and **HL¹**−**HL⁶** were determined by the traditional shake-flask method in *n*-octanol/buffered aqueous solution at pH 7.40 (20 mM HEPES, 0.10 M KCl) at 25.0 ± 0.2 °C as described previously.[82]

5.7. Crystallographic Structure Determination. X-ray diffraction quality single crystals of **HL¹**, **HL²**, and **HL⁴**−**HL⁶** were obtained by recrystallization in ethanol, while **1** and **3**−**6** by slow diffusion of diethyl ether into the DMF and methanolic solution of the complexes, respectively. The measurements were performed on a Bruker X8 APEX-II CCD (**HL¹**, **HL²**, **HL⁴**, **HL⁵**, **1′**, **3**−**6**), Bruker D8 Venture (**1**), or Gemini (**HL⁶**) diffractometer. Single crystals were positioned at 35, 35, 35, 35, and 55 mm from the detector, and 388, 1110, 946, 1108, and 2935 frames were measured, each for 40, 3, 60, 3, and 32 s over 0.5°, 0.5°, 0.5°, 0.5°, and 1.0° scan width for **HL¹**, **HL²**, and **HL⁴**−**HL⁶**, respectively. For Cu(II) complexes **1**, **1′**, **3**−**6** the single crystals were placed at 24, 35, 35, 33, 35, and 24 mm from the detector, and 8088, 2692, 794, 1212, 1261, and 567 fames were measured, each for 3, 2, 60, 60, 60, and 3 s over 0.6°, 0.5°, 0.5°, 0.5°, 0.4°, and 0.5° scan width, respectively. The data were processed using SAINT or CrysAlis software.[83,84] Crystal data, data collection

DOI: 10.1021/acs.jmedchem.8b01031
J. Med. Chem. 2019, 62, 512−530

parameters, and structure refinement details are given in Tables S11 and S12. The structures were solved by direct methods and refined by full-matrix least-squares techniques. Non-H atoms were refined with anisotropic displacement parameters. H atoms were inserted in calculated positions and refined with a riding model. The morpholine group and the *N*-piperidinyl unit in one of three crystallographically independent molecules in the asymmetric unit were found to be disordered over two positions with s.o.f. 0.5:0.5 and 0.6:0.4 in **3·0.25MeOH**. The morpholine moiety attached to pyridine unit in one of the three crystallographically independent molecules of **4·0.58MeOH** was found to be disordered over two positions with s.o.f. 0.7:0.3. In addition, one molecule of methanol was found disordered over two positions with s.o.f. 0.75:0.25. The positional parameters of disordered atoms were refined by using PART, DFIX, and SADI tools implemented in SHELX. The following computer programs and hardware were used: structure solution, *SHELXS-2014* and refinement, *SHELXL-2014*;[85] molecular diagrams, and ORTEP;[86] computer, Intel CoreDuo. CCDC 1850567−1850577.

5.8. Electrochemistry and Spectroelectrochemistry. Cyclic voltammetric experiments were performed as described previously.[46] The cyclic voltammograms were measured in the cathodic region in different solvents (DMSO, methanol, DMSO/H_2O). The analytical purity grade $LiClO_4$ (Sigma-Aldrich) and distilled and deionized water were used for preparation of 1 mM aqueous solutions of the investigated complexes **1**−**6**. EPR spectra were recorded with the EMX plus. In situ UV−vis−NIR spectroelectrochemical measurements were performed on a spectrometer (Avantes, Model AvaSpec-2048x14-USB2 in the spectroelectrochemical cell kit (AKSTCKIT3)) with the Pt-microstructured honeycomb working electrode, purchased from Pine Research Instrumentation. The cell was positioned in the CUV−UV Cuvette Holder (Ocean Optics) connected to the diode-array UV−vis−NIR spectrometer by optical fibers. UV−vis−NIR spectra were processed using the AvaSoft 7.7 software package. Halogen and deuterium lamps were used as light sources (Avantes, Model AvaLight-DH-S-BAL). The in situ EPR spectroelectrochemical experiments were carried out under an argon atmosphere in the EPR flat cell equipped with a large platinum mesh working electrode. The freshly prepared solutions were carefully purged with argon and the electrolytic cell was polarized in the galvanostatic mode directly in the cylindrical EPR cavity TM-110 (ER 4103 TM), and the EPR spectra were measured in situ.

5.9. Cell Lines and Culture Conditions. Human ovarian carcinoma cells A2780 and A2780cisR and human embryonic kidney HEK293 were obtained from ATCC. A2780 and A2780cisR cells were cultured in RPMI 1640 medium containing 10% FBS. HEK293 were cultured in DMEM medium containing 10% FBS. All cells were grown in tissue culture 25 cm^2 flasks (BD Biosciences, Singapore) at 37 °C in a humidified atmosphere of 95% air and 5% CO_2. All drug stock solutions were prepared in sterile water. The amount of Cu was determined by ICP−OES. All compounds were soluble in water; more specifically, the solubility of **1**, **2**, and **5** was moderate and did not exceed 2 mM, whereas **3** was less soluble (0.3 mM) in water.

5.10. Inhibition of Cell Viability Assay. The cytotoxicity of the compounds was determined by colorimetric microculture assay (MTT assay, MTT = 3-(4,5-dimethyl-2-thiazolyl)-2,5-diphenyl-2*H*-tetrazolium bromide) as described previously.[46]

5.11. Cellular Accumulation. Cellular accumulation of **1**−**6** was determined in A2780 cells. Cells were seeded into Cellstar 6-well plates (Greiner Bio-one) at a density of 60 × 10^4 cells/well (2 mL per well). After the cells were allowed to resume exponential growth for 24 h, they were exposed to **1**−**6** at 1 μM for 24 h at 37 °C. The cells were washed twice with 1 mL of PBS and lysed with RIPA lysis buffer for 5−10 min at 4 °C. The cell lysates were scraped from the wells and transferred to separate 1.5 mL microtubes. The supernatant was then collected after centrifugation (13 000 rpm, 4 °C for 15 min) and total protein content of each sample was quantified via Bradford's assay. Cell lysates were transferred to 2 mL glass vials and then digested with ultrapure 65% HNO_3 at 100 °C for 24 h. The resulting solution was diluted to 1 mL (2−4% v/v HNO_3) with ultrapure Milli-Q water. Cu content of each sample was quantified by ICP−MS. In was used as an internal standard. Cu and In were measured at m/z 64 and m/z 115, respectively. Metal standards for calibration curve (0, 0.5, 1, 2, 5, 10, 20, and 40 ppb) were freshly prepared before each measurement. All readings were made in triplicates in He mode. For temperature-dependent cellular accumulation experiments, A2780 cells were seeded into 35 n 10 mm tissue culture plates at a density of 60 0 10^4 cells/plate. After the cells were allowed to resume exponential growth for 24 h, they were exposed to **2** at 3 μM for 10, 30, 60, and 120 min at 37 and 4 °C. The subsequent analysis was performed as described above. For energy-dependent experiments, A2780 cells were seeded into 35 5 10 mm tissue culture plates at a density of 1 0 10^6 cells/plate. After the cells were allowed to resume exponential growth for 24 h, they were preincubated with oligomycin (5 μM) for 1 or 4 h or with cycloheximide (100 μM) for 4 h and further co-incubated with 3 μM of **2** at 37 °C. To induce total starvation, after the cells were allowed to resume exponential growth for 24 h, RPMI media was replaced with HBSS, and cells were preincubated in HBSS for 1 h and further incubated with 3 μM of **2** for 1 h at 37 °C. The subsequent analysis was performed as described above.

5.12. Western Blot Analysis. A2780 cells were seeded into Cellstar 6-well plates (Greiner Bio-One) at a density of 60 × 10^4 cells/well (2 mL per well). After the cells were allowed to resume exponential growth for 24 h, they were exposed to HL^2 and **2** at different concentrations for 24 h. The experiment was performed essentially as described previously.[46] The membranes were blocked in 5% BSA (w/v) in TBST wash buffer for 1 h and subsequently incubated with the appropriate primary antibodies in 5% BSA (w/v) in TBST wash buffer (actin antibody) at 4 °C overnight. The membranes were washed with a wash buffer three times for 5 min. After incubation with horseradish peroxidase-conjugated secondary antibodies (room temperature, 1.5 h), the membranes were washed with a wash buffer four times for 5 min. Immune complexes were detected with Luminata HRP substrates and analyzed using enhanced chemiluminescence imaging. Actin was used as a loading control. The following antibodies were used: NRF2 (sc13032) from Santa Cruz Biotechnologies, ECL Antirabbit IgG (NA934 V), and ECL Antimouse IgG (NA931) from GE Healthcare Life Sciences, cleaved PARP (Asp214) (D64E10), PARP, CHOP (D46F1), BiP (C50B12), IRE1α (14C10), β-actin (13E5), phospho-p44/p42 MAPK (Erk1/2) (Thr202/Tyr204) (D13.14.4E), cyclin D1 (92G2), cyclin B1 (D5C10), and XIAP antibodies from Cell Signalling Technologies. All antibodies were used at 1:500 dilutions except for actin (1:10 000), antimouse and antirabbit (1:5000).

5.13. Annexin V/PI Apoptosis Assay. A2780 cells were seeded into Cellstar 12-well plates (Greiner Bio-One) at a density of 20 × 10^4 cells/well (1 mL per well). The cells were allowed to resume exponential growth for 24 h and subsequently they were exposed to HL^2 and **2** at different concentrations for 24 h. After the supernatant solution was collected in 1.5 mL microtubes, the cells were washed with 100 μL of trypsin, which was combined with the supernatant. Subsequently, cells were trypsinized with 200 μL of trypsin for 5 min at 37 °C, 5% CO_2, washed with 200 μL of PBS, and combined with the supernatant. The cells were centrifuged at 2.5 × 10^3 rpm for 5 min and the pellets were washed once with PBS and resuspended in 500 μL of Annexin V binding buffer and stained with Annexin V-FITC and PI reagents. The fluorescence was immediately analyzed by flow cytometry. The resulting dot blots were acquired from 10 000 events and quantified using Flowjo software (Flowjo LLC, Ashland, OR, USA).

5.14. Tyrosyl Radical Reduction in Mouse R2 Ribonucleotide Reductase Protein. The 9.4 GHz EPR spectra were recorded at 30 K on a Bruker EleXsys II E540 EPR spectrometer with an Oxford Instruments ESR900 helium cryostat, essentially as described previously.[51] The mouse R2 subunit was produced from *Escherichia coli* carrying a mouse R2 cDNA plasmid. The protein was reconstituted with Fe, resulting in the formation of the cluster with 0.38 tyrosyl radical/Fe per monomer, which is in agreement with the literature.[41]

DOI: 10.1021/acs.jmedchem.8b01031
J. Med. Chem. 2019, 62, 512−530

5.15. Molecular Docking Calculations. The calculations were performed as described previously.[20] The center of the binding pocket was defined (x = 102.276, y = 87.568, z = 80.588) with 10 Å radius. The basic amino acids lysine and arginine were defined as protonated. Furthermore, aspartic and glutamic acids were assumed to be deprotonated. The GoldScore (GS),[37] ChemScore (CS),[88,89] Chem Piecewise Linear Potential (ChemPLP),[90] and Astex Statistical Potential (ASP)[87] scoring functions were implemented to validate the predicted binding modes and relative energies of the ligands using the GOLD v5.4 software suite. The parameter file for GS was augmented for Cu according to Sciortino et al.[38] The QikProp 4.6[91] and Marvin software package[92] was used to calculate the molecular descriptors of the compounds. The reliability of QikProp is established for the molecular descriptors.[93]

5.16. Bacterial Strains and Antibacterial Activity. Wild-type *P. aeruginosa* PAO1 strain CECT 4122 (ATCC 15692) and *S. aureus* CECT 86 (ATCC 12600) were obtained from the Spanish Type Culture Collection (CECT). All strains were routinely cultivated in TSB medium (Sharlab, Spain) at 37 °C. MIC assays were determined by the microdilution method using TSB broth following the method described by the Clinical and Laboratory standards Institute.[94] In brief, compounds were diluted in a 96-well microtiter plate (tissue culture-treated polystyrene; Costar 3595, Corning Inc., Corning, NY) to a final concentration ranging from 0.1 to 100 μg/mL. A 100 μL aliquot of the bacterial suspension (around 5 × 10^5 cfu/mL) was inoculated, incubated at 37 °C for 8 h at 150 rpm, and absorbance at 550 nm was read every 15 min in an Infinity 200 Pro microplate reader (Tecan). The MIC_{100} was determined as the lowest concentration that completely inhibited bacterial growth and MIC_{50} in which bacterial growth was inhibited at 50%.

5.17. Bacterial Viability Test Analysis. Cultures of *S. aureus* and *P. aeruginosa* were diluted in fresh TSB medium and grown overnight to the beginning of exponential phase (A550 0.3), and different compounds were added. After 3 h of incubation at 37 °C in shaking conditions, cells were harvested and stained using the LIVE/DEAD BactLight Bacterial Viability Kit (Thermofisher) for 30 min. Fluorescent bacteria were visualized by a Nikon inverted fluorescent microscope ELIPSE Ti-S/L100 (Nikon) coupled with a DS-Qi2 Nikon camera.

■ ASSOCIATED CONTENT

Supporting Information

The Supporting Information is available free of charge on the ACS Publications website at DOI: 10.1021/acs.jmedchem.8b01031.

Synthetic details, atom numbering scheme for NMR spectra, ORTEP views of **HL**[1], **HL**[2], **HL**[4−6], portion of the crystal structure of **6**, low field region of the ^{1}H NMR spectra of **HL**[1] recorded at pH 0.75−12.50, concentration distribution curves of **HL**[1], UV−vis and EPR spectra for Cu(II) containing systems, cyclic voltammograms and UV−vis spectra of **1**−**6** and one of the proligands, plot with potential dependence of UV−vis spectra of **2**, concentration−effect curves, hydrogen binding of **5** to R2 protein, EPR spectrum of R2 RNR tyrosyl radical, complex formation reactions of Fe^{III} and Fe^{II} with **HL**[2] and **HL**[5] monitored by UV−vis spectroscopy, ESI MS spectrum of $[Fe^{III}(HL^5)]^+$, selected bond distances and angles in Cu(I) complexes, proton dissociation constants for **HL**[1], cumulative stability and proton dissociation constants of Cu(II) complexes of HL, formation constants for Cu(II)−**HL**[1] complexes, electrochemical data for **1**−**6**, molecular descriptors for **HL**[1]−**HL**[6] and **1**−**6**, details of molecular docking calculations, analytical data, and details of data collection and refinement of proligands and Cu(II) complexes (PDF)

Molecular formula strings (CSV)

(PDB)

checkCIF (basic structural check) running, datablock: elaf009 (PDF)

checkCIF (basic structural check) running, datablock: elaf011 (PDF)

checkCIF (basic structural check) running, datablock: elaf012 (PDF)

checkCIF (basic structural check) running, datablock: elaf015 (PDF)

checkCIF (basic structural check) running, datablock: elaf016 (PDF)

checkCIF (basic structural check) running, datablock: elaf017 (PDF)

checkCIF (basic structural check) running, datablock: elaf023 (PDF)

checkCIF (basic structural check) running, datablock: exp1427 (PDF)

checkCIF (basic structural check) running, datablock: feba391 (PDF)

checkCIF (basic structural check) running, datablock: kaoh444 (PDF)

checkCIF (basic structural check) running, datablock: kaoh503 (PDF)

Crystallographic data (CIF)

Crystallographic data (CIF)

Crystallographic data (CIF)

Crystallographic data (CIF)

Crystallographic data (CIF)

Crystallographic data (CIF)

Crystallographic data (CIF)

Crystallographic data (CIF)

Crystallographic data (CIF)

Crystallographic data (CIF)

Crystallographic data (CIF)

Accession Codes

PDB ID of the complexes of triapine and **5** docked in mouse R2 protein: 1w68-5-T. Authors will release the atomic coordinates upon article publication.

■ AUTHOR INFORMATION

Corresponding Authors

*E-mail: maria.babak@nus.edu.sg.

*E-mail: vladimir.arion@univie.ac.at.

ORCID

Eduard Torrents: 0000-0002-3010-1609

Nóra V. May: 0000-0003-4770-4681

Ana Popović-Bijelić: 0000-0003-3121-2391

Maria V. Babak: 0000-0002-2009-7837

Giorgia Pastorin: 0000-0002-2568-0626

Vladimir B. Arion: 0000-0002-1895-6460

Author Contributions

[††]K.O. and E.A. contributed equally.

Notes

The authors declare no competing financial interest.

■ ACKNOWLEDGMENTS

Austrian Science Fund (FWF) is acknowledged for the grant no. P28223-N34. This work was supported in part by grants to

E.T. from the Spanish Ministerio de Economia y Competitividad (MINECO/FEDER) (BIO2015-63557-R), Generalitat de Catalunya (2014 SGR01260 and CERCA programme), the Catalan and Spanish Cystic Fibrosis foundations and La Caixa Foundation. This work was also supported by the National Research, Development and Innovation Office FK 124240 project, and the J. Bolyai Research Scholarship of the Hungarian Academy of Sciences (ÉAE and NVM). P.R. and D.D. acknowledge the support of Slovak Research and Development Agency (APVV-15-0053) and Slovak Scientific Grant Agency VEGA (1/0416/17). This work was supported by the National University of Singapore (NUS), Department of Pharmacy (C148-000-003-001 (FYP)). We thank A. Roller for collection of X-ray data.

■ ABBREVIATIONS

TSC, thiosemicarbazone; COTI-2, (*E*)-*N*′-(6,7-dihydroquinolin-8(5*H*)-ylidene)-4-(pyridine-2-yl)piperazine-1-carbothiohydrazide; DpC, di-2-pyridylketone 4-cyclohehyl-4-methyl-3-thiosemicarbazone; ROS, reactive oxygen species; GSH, glutathione; UPR, unfolded protein response; TEMED, tetramethylethylenediamine; PI, propidium iodide; FBS, fetal bovine serum; BSA, bovine serum albumin; HBSS, Hank's Balanced Salt Solution; PS, phosphatidylserine; KDS, known drug space

■ REFERENCES

(1) Chabner, B. A.; Roberts, T. G. Chemotherapy and the war on cancer. *Nat. Rev. Cancer* **2005**, *5*, 65−72.
(2) Inagaki, J.; Rodriguez, V.; Bodey, G. P. Causes of death in cancer patients. *Cancer* **1974**, *33*, 568−573.
(3) Alibek, K.; Bekmurzayeva, A.; Mussabekova, A.; Sultankulov, B. Using antimicrobial adjuvant therapy in cancer treatment: a review. *Infect. Agents Cancer* **2012**, *7*, 33.
(4) Kardas, J.; Buraczewska, A. The use of antibiotic profilaxis in patients with solid tumours − when and to whom? *Oncol. Clin. Pract.* **2016**, *6*, 128−135.
(5) Benharroch, D.; Osyntsov, L. Infectious diseases are analogous with cancer. Hypothesis and implications. *J. Cancer* **2012**, *3*, 117−121.
(6) Elledge, S. J.; Zhou, Z.; Allen, J. B. Ribonucleotide reductase: regulation, regulation, regulation. *Trends Biochem. Sci.* **1992**, *17*, 119−123.
(7) Torrents, E. Ribonucleotide reductases: essential enzymes for bacterial life. *Front. Cell. Infect. Microbiol.* **2014**, *4*, 52.
(8) Beraldo, H.; Gambino, D. The wide pharmacological versatility of semicarbazones, thiosemicarbazones and their metal complexes. *Mini-Rev. Med. Chem.* **2004**, *4*, 31−39.
(9) Knox, J. J.; Hotte, S. J.; Kollmannsberger, C.; Winquist, E.; Fisher, B.; Eisenhauer, E. A. Phase II study of Triapine in patients with metastatic renal cell carcinoma: a trial of the National Cancer Institute of Canada Clinical Trials Group (NCIC IND.161). *Invest. New Drugs* **2007**, *25*, 471−477.
(10) Nutting, C. M.; van Herpen, C. M. L.; Miah, A. B.; Bhide, S. A.; Machiels, J.-P.; Buter, J.; Kelly, C.; de Raucourt, D.; Harrington, K. J. Phase II study of 3-AP Triapine in patients with recurrent or metastatic head and neck squamous cell carcinoma. *Ann. Oncol.* **2009**, *20*, 1275−1279.
(11) Traynor, A. M.; Lee, J.-W.; Bayer, G. K.; Tate, J. M.; Thomas, S. P.; Mazurczak, M.; Graham, D. L.; Kolesar, J. M.; Schiller, J. H. A phase II trial of Triapine (NSC# 663249) and Gemcitabine as second line treatment of advanced non-small cell lung cancer: Eastern Cooperative Oncology Group study 1503. *Invest. New Drugs* **2009**, *28*, 91−97.
(12) Stacy, A. E.; Palanimuthu, D.; Bernhardt, P. V.; Kalinowski, D. S.; Jansson, P. J.; Richardson, D. R. Structure-activity relationships of di-2-pyridylketone, 2-benzoylpyridine, and 2-acetylpyridine thiosemicarbazones for overcoming Pgp-mediated drug resistance. *J. Med. Chem.* **2016**, *59*, 8601−8620.
(13) https://clinicaltrials.gov/ct2/show/NCT02688101 (accessed Feb 23, 2016).
(14) Salim, K. Y.; Danter, W. R.; Vareki, S. M.; Koropatnick, J. COTI-2, a novel small molecule that is active against multiple human cancer cell lines in vitro and in vivo. *Oncotarget* **2016**, *7*, 41363−41379.
(15) West, D. X.; Liberta, A. E.; Padhye, S. B.; Chikate, R. C.; Sonawane, P. B.; Kumbhar, A. S.; Yerande, R. G. Thiosemicarbazone complexes of copper(II): structural and biological studies. *Coord. Chem. Rev.* **1993**, *123*, 49−71.
(16) Bacher, F.; Dömötör, O.; Kaltenbrunner, M.; Mojović, M.; Popović-Bijelić, A.; Gräslund, A.; Ozarowski, A.; Filipovic, L.; Radulović, S.; Enyedy, É. A.; Arion, V. B. Effects of terminal dimethylation and metal coordination of proline-2-formylpyridine thiosemicarbazone hybrids on lipophilicity, antiproliferative activity, and hR2 RNR inhibition. *Inorg. Chem.* **2014**, *53*, 12595−12609.
(17) Milunovic, M. N. M.; Enyedy, É. A.; Nagy, N. V.; Kiss, T.; Trondl, R.; Jakupec, M. A.; Keppler, B. K.; Krachler, R.; Novitchi, G.; Arion, V. B. L- and D-proline thiosemicarbazone conjugates: coordination behavior in solution and the effect of copper(II) coordination on their antiproliferative activity. *Inorg. Chem.* **2012**, *51*, 9309−9321.
(18) Bacher, F.; Dömötör, O.; Chugunova, A.; Nagy, N. V.; Filipović, L.; Radulović, S.; Enyedy, É. A.; Arion, V. B. Strong effect of copper(II) coordination on antiproliferative activity of thiosemicarbazone-piperazine and thiosemicarbazone-morpholine hybrids. *Dalton Trans.* **2015**, *44*, 9071−9090.
(19) Dobrova, A.; Platzer, S.; Bacher, F.; Milunovic, M. N. M.; Dobrov, A.; Spengler, G.; Enyedy, É. A.; Novitchi, G.; Arion, V. B. Structure-antiproliferative activity studies on l-proline- and homoproline-4-N-pyrrolidine-3-thiosemicarbazone hybrids and their nickel(II), palladium(II) and copper(II) complexes. *Dalton Trans.* **2016**, *45*, 13427−13439.
(20) Zaltariov, M. F.; Hammerstad, M.; Arabshahi, H. J.; Jovanović, K.; Richter, K. W.; Cazacu, M.; Shova, S.; Balan, M.; Andersen, N. H.; Radulović, S.; Reynisson, J.; Andersson, K. K.; Arion, V. B. New iminodiacetate-thiosemicarbazone hybrids and their copper(II) complexes are potential ribonucleotide reductase R2 inhibitors with high antiproliferative activity. *Inorg. Chem.* **2017**, *56*, 3532−3549.
(21) Naim, M. J.; Alam, O.; Alam, M. J.; Alam, P.; Shrivastava, N. A review on pharmacological profile of morpholine derivatives. *Int. J. Pharmacol. Pharm. Sci.* **2016**, *3*, 40−51.
(22) Boehm, M. F.; Heyman, R. A. Compounds Having Selective Activity for Retinoid X Receptors, and Means for Modulation of Processes Mediated by Retinoid X Receptors. U.S. Patent 7,655,699 B1, 2010.
(23) Warr, R. J.; Willis, A. C.; Wild, S. B. Inorganic asymmetric synthesis: asymmetric synthesis of a two-bladed propeller, octahedral metal complex. *Inorg. Chem.* **2006**, *45*, 8618−8627.
(24) Dawson, M. I.; Chan, R.; Hobbs, P. D.; Chao, W.; Schiff, L. J. Aromatic retinoic acid analogs. 2. Synthesis and pharmacological activity. *J. Med. Chem.* **1983**, *26*, 1282−1293.
(25) Dömötör, O.; May, N. V.; Pelivan, K.; Kiss, T.; Keppler, B. K.; Kowol, C. R.; Enyedy, É. A. A comparative study of α-*N*-pyridyl thiosemicarbazones: Spectroscopic properties, solution stability and copper(II) complexation. *Inorg. Chim. Acta* **2018**, *472*, 264−275.
(26) Enyedy, É. A.; Zsigó, É.; Nagy, N. V.; Kowol, C. R.; Roller, A.; Keppler, B. K.; Kiss, T. Complex-Formation Ability of Salicylaldehyde Thiosemicarbazone towards Zn^{II}, Cu^{II}, Fe^{II}, Fe^{III} and Ga^{III} Ions. *Eur. J. Inorg. Chem.* **2012**, *2012*, 4036−4047.
(27) Kowol, C. R.; Heffeter, P.; Miklos, W.; Gille, L.; Trondl, R.; Cappellacci, L.; Berger, W.; Keppler, B. K. Mechanisms underlying reductant-induced reactive oxygen species formation by anticancer copper(II) compounds. *J. Biol. Inorg Chem.* **2011**, *17*, 409−423.
(28) Göschl, S.; Varbanov, H. P.; Theiner, S.; Jakupec, M. A.; Galanski, M.; Keppler, B. K. The role of the equatorial ligands for the

DOI: 10.1021/acs.jmedchem.8b01031
J. Med. Chem. 2019, 62, 512−530

redox behavior, mode of cellular accumulation and cytotoxicity of platinum(IV) prodrugs. *J. Inorg. Biochem.* **2016**, *160*, 264−274.
(29) Primik, M. F.; Mühlgassner, G.; Jakupec, M. A.; Zava, O.; Dyson, P. J.; Arion, V. B.; Keppler, B. K. Highly cytotoxic copper(II) complexes with modified paullone ligands. *Inorg. Chem.* **2010**, *49*, 302−311.
(30) Waring, M. J. Lipophilicity in drug discovery. *Expert Opin. Drug Discovery* **2010**, *5*, 235−248.
(31) Zhu, F.; Logan, G.; Reynisson, J. Wine compounds as a source for HTS screening collections. A feasibility study. *Mol. Inf.* **2012**, *31*, 847−855.
(32) Los, D. A.; Murata, N. Membrane fluidity and its roles in the perception of environmental signals. *Biochim. Biophys. Acta, Biomembr.* **2004**, *1666*, 142−157.
(33) Price, K. A.; Crouch, P. J.; Volitakis, I.; Paterson, B. M.; Lim, S.; Donnelly, P. S.; White, A. R. Mechanisms controlling the cellular accumulation of copper bis(thiosemicarbazonato) complexes. *Inorg. Chem.* **2011**, *50*, 9594−9605.
(34) Merlot, A. M.; Pantarat, N.; Menezes, S. V.; Sahni, S.; Richardson, D. R.; Kalinowski, D. S. Cellular uptake of the antitumor agent Dp44mT occurs via a carrier/receptor-mediated mechanism. *Mol. Pharmacol.* **2013**, *84*, 911−924.
(35) Sugano, K.; Kansy, M.; Artursson, P.; Avdeef, A.; Bendels, S.; Di, L.; Ecker, G. F.; Faller, B.; Fischer, H.; Gerebtzoff, G.; Lennernaes, H.; Senner, F. Coexistence of passive and carrier-mediated processes in drug transport. *Nat. Rev. Drug Discovery* **2010**, *9*, 597−614.
(36) Strand, K. R.; Karlsen, S.; Kolberg, M.; Røhr, Å. K.; Görbitz, C. H.; Andersson, K. K. Crystal structural studies of changes in the native dinuclear iron center of ribonucleotide reductase protein R2 from mouse. *J. Biol. Chem.* **2004**, *279*, 46794−46801.
(37) Jones, G.; Willett, P.; Glen, R. C.; Leach, A. R.; Taylor, R. Development and validation of a genetic algorithm for flexible docking. *J. Mol. Biol.* **1997**, *267*, 727−748.
(38) Sciortino, G.; Rodríguez-Guerra Pedregal, J.; Lledós, A.; Garribba, E.; Maréchal, J.-D. Prediction of the interaction of metallic moieties with proteins: an update for protein-ligand docking techniques. *J. Comput. Chem.* **2017**, *39*, 42−51.
(39) Gräslund, A.; Ehrenberg, A.; Thelander, L. Characterisation of the free radical of mammalian ribonucleotide reductase. *J. Biol. Chem.* **1982**, *257*, 5711−5715.
(40) Thelander, L.; Graslund, A. Mechanism of inhibiton of mammalian ribonucleotide reductase by the iron chelate of 1-formylisoquinonline thiosemicarbazone. *J. Biol. Chem.* **1983**, *258*, 4063−4066.
(41) Popović-Bijelić, A.; Kowol, C. R.; Lind, M. E. S.; Luo, J.; Himo, F.; Enyedy, E. A.; Arion, V. B.; Gräslund, A. Ribonucleotide reductase inhibition by metal complexes of Triapine (3-aminopyridine-2-carboxaldehyde thiosemicarbazone): a combined experimental and theoretical study. *J. Inorg. Biochem.* **2011**, *105*, 1422−1431.
(42) Enyedy, É. A.; Primik, M. F.; Kowol, C. R.; Arion, V. B.; Kiss, T.; Keppler, B. K. Interaction of Triapine and related thiosemicarbazones with iron(III)/(II) and gallium(III): a comparative solution equilibrium study. *Dalton Trans.* **2011**, *40*, 5895−5905.
(43) Mullen, P. PARP cleavage as a means of assessing apoptosis. *Methods Mol. Med.* **2004**, *88*, 171−181.
(44) Finch, R. A.; Liu, M.-C.; Cory, A. H.; Cory, J. G.; Sartorelli, A. C. Triapine (3-aminopyridine-2-carboxaldehyde thiosemicarbazone; 3-AP): an inhibitor of ribonucleotide reductase with antineoplastic activity. *Adv. Enzyme Regul.* **1999**, *39*, 3−12.
(45) Finch, R. A.; Liu, M.-C.; Grill, S. P.; Rose, W. C.; Loomis, R.; Vasquez, K. M.; Cheng, Y.-C.; Sartorelli, A. C. Triapine (3-aminopyridine-2-carboxaldehyde- thiosemicarbazone): A potent inhibitor of ribonucleotide reductase activity with broad spectrum antitumor activity. *Biochem. Pharmacol.* **2000**, *59*, 983−991.
(46) Yu, Y.; Wong, J.; Lovejoy, D. B.; Kalinowski, D. S.; Richardson, D. R. Chelators at the Cancer Coalface: Desferrioxamine to Triapine and Beyond. *Clin. Cancer Res.* **2006**, *12*, 6876−6883.
(47) Shao, J.; Zhou, B.; Di Bilio, A. J.; Zhu, L.; Wang, T.; Qi, C.; Shih, J.; Yen, Y. A ferrous-triapine complex mediates formation of reactive oxygen species that inactivate human ribonucleotide reductase. *Mol. Cancer Ther.* **2006**, *5*, 586−592.
(48) Kowol, C. R.; Trondl, R.; Heffeter, P.; Arion, V. B.; Jakupec, M. A.; Roller, A.; Galanski, M.; Berger, W.; Keppler, B. K. Impact of Metal Coordination on Cytotoxicity of 3-Aminopyridine-2-carboxaldehyde Thiosemicarbazone (Triapine) and Novel Insights into Terminal Dimethylation. *J. Med. Chem.* **2009**, *52*, 5032−5043.
(49) Yu, Y.; Gutierrez, E.; Kovacevic, Z.; Saletta, F.; Obeidy, P.; Suryo Rahmanto, Y.; Richardson, D. R. Iron chelators for the treatment of cancer. *Curr. Med. Chem.* **2012**, *19*, 2869−2702.
(50) Merlot, A. M.; Kalinowski, D. S.; Richardson, D. R. Novel chelators for cancer treatment: where are we now? *Antioxid. Redox Signaling* **2013**, *18*, 973−1006.
(51) Aye, Y.; Long, M. J. C.; Stubbe, J. Mechanistic Studies of Semicarbazone Triapine Targeting Human Ribonucleotide Reductasein Vitroand in Mammalian Cells. *J. Biol. Chem.* **2012**, *287*, 35768−35778.
(52) Pandeya, S. N.; Sriram, D.; Nath, G.; DeClercq, E. Synthesis, antibacterial, antifungal and anti-HIV activities of Schiff and Mannich bases derived from isatin derivatives and N-[4-(4′-chlorophenyl)-thiazol-2-yl] thiosemicarbazide. *Eur. J. Pharm. Sci.* **1999**, *9*, 25.
(53) Sîrbu, A.; Palamarciuc, O.; Babak, M. V.; Lim, J. M.; Ohui, K.; Enyedy, E. A.; Shova, S.; Darvasiová, D.; Rapta, P.; Ang, W. H.; Arion, V. B. Copper(II) thiosemicarbazone complexes induce marked ROS accumulation and promote nrf2-mediated antioxidant response in highly resistant breast cancer cells. *Dalton Trans.* **2017**, *46*, 3833−3847.
(54) Yu, Y.; Kalinowski, D. S.; Kovacevic, Z.; Siafakas, A. R.; Jansson, P. J.; Stefani, C.; Lovejoy, D. B.; Sharpe, P. C.; Bernhardt, P. V.; Richardson, D. R. Thiosemicarbazones from the old to new: iron chelators that are more than just ribonucleotide reductase inhibitors. *J. Med. Chem.* **2009**, *52*, 5271−5294.
(55) Antholine, W.; Knight, J.; Whelan, H.; Petering, D. H. Studies of the reaction of 2-formylpyridine thiosemicarbazone and its iron and copper complexes with biological systems. *Mol. Pharmacol.* **1977**, *13*, 89−98.
(56) Chaston, T. B.; Lovejoy, D. B.; Watts, R. N.; Richardson, D. R. Examination of the antiproliferative activity of iron chelators: multiple cellular targets and the different mechanism of action of triapine compared with desferrioxamine and the potent pyridoxal isonicotinoyl hydrazone analogue 311. *Clin Cancer Res* **2003**, *9*, 402−414.
(57) Yu, Y.; Kovacevic, Z.; Richardson, D. R. Tuning cell cycle regulation with an iron key. *Cell Cycle* **2014**, *6*, 1982−1994.
(58) Nurtjahja-Tjendraputra, E.; Fu, D.; Phang, J. M.; Richardson, D. R. Iron chelation regulates cyclin D1 expression via the proteasome: a link to iron deficiency-mediated growth suppression. *Blood* **2006**, *109*, 4045−4054.
(59) Thelander, L.; Gräslund, A.; Thelander, M. Continual presence of oxygen and iron required for mammalian ribonucleotide reduction: Possible regulation mechanism. *Biochem. Biophys. Res. Commun.* **1983**, *110*, 859−865.
(60) Lui, G. Y. L.; Kovacevic, Z.; Menezes, S. V.; Kalinowski, D. S.; Merlot, A. M.; Sahni, S.; Richardson, D. R. Novel thiosemicarbazones regulate the signal transducer and activator of transcription 3 (STAT3) pathway: inhibition of constitutive and interleukin 6-induced activation by iron depletion. *Mol. Pharmacol.* **2015**, *87*, 543−560.
(61) Yu, Y.; Rahmanto, Y. S.; Richardson, D. R. Bp44mT: an orally active iron chelator of the thiosemicarbazone class with potent anti-tumour efficacy. *Br. J. Pharmacol.* **2011**, *165*, 148−166.
(62) Karin, M. The regulation of AP-1 activity by mitogen-activated protein kinases. *J. Biol. Chem.* **1995**, *270*, 16483−16486.
(63) Lee, S.-K.; Jang, H.-J.; Lee, H.-J.; Lee, J.; Jeon, B.-H.; Jun, C.-D.; Lee, S.-K.; Kim, E.-C. p38 and ERK MAP kinase mediates iron chelator-induced apoptosis and -suppressed differentiation of immortalized and malignant human oral keratinocytes. *Life Sci.* **2006**, *79*, 1419−1427.
(64) Moon, S.-K.; Jung, S.-Y.; Choi, Y.-H.; Lee, Y.-C.; Patterson, C.; Kim, C.-H. PDTC, metal chelating compound, induces G1 phase cell

DOI: 10.1021/acs.jmedchem.8b01031
J. Med. Chem. 2019, 62, 512−530

cycle arrest in vascular smooth muscle cells through inducing p21Cip1 expression: Involvement of p38 mitogen activated protein kinase. *J. Cell. Physiol.* **2003**, *198*, 310−323.
(65) Lane, D. J. R.; Mills, T. M.; Shafie, N. H.; Merlot, A. M.; Saleh Moussa, R.; Kalinowski, D. S.; Kovacevic, Z.; Richardson, D. R. Expanding horizons in iron chelation and the treatment of cancer: role of iron in the regulation of ER stress and the epithelial-mesenchymal transition. *Biochim. Biophys. Acta, Rev. Cancer* **2014**, *1845*, 166−181.
(66) Lane, D. J. R.; Saletta, F.; Rahmanto, Y. S.; Kovacevic, Z.; Richardson, D. R. N-myc downstream regulated 1 (NDRG1) is regulated by eukaryotic initiation factor 3a (eIF3a) during cellular stress caused by iron depletion. *PLoS One* **2013**, *8*, e57273.
(67) Trondl, R.; Flocke, L. S.; Kowol, C. R.; Heffeter, P.; Jungwirth, U.; Mair, G. E.; Steinborn, R.; Enyedy, E. A.; Jakupec, M. A.; Berger, W.; Keppler, B. K. Triapine and a more potent dimethyl derivative induce endoplasmic reticulum stress in cancer cells. *Mol. Pharmacol.* **2013**, *85*, 451−459.
(68) Merlot, A. M.; Shafie, N. H.; Yu, Y.; Richardson, V.; Jansson, P. J.; Sahni, S.; Lane, D. J. R.; Kovacevic, Z.; Kalinowski, D. S.; Richardson, D. R. Mechanism of the induction of endoplasmic reticulum stress by the anti-cancer agent, di-2-pyridylketone 4,4-dimethyl-3-thiosemicarbazone (Dp44mT): Activation of PERK/eIF2α, IRE1α, ATF6 and calmodulin kinase. *Biochem. Pharmacol.* **2016**, *109*, 27−47.
(69) Fu, Y.; Liu, Y.; Wang, J.; Li, C.; Zhou, S.; Yang, Y.; Zhou, P.; Lu, C.; Li, C. Calcium release induced by 2-pyridinecarboxaldehyde thiosemicarbazone and its copper complex contributes to tumor cell death. *Oncol. Rep.* **2017**, *37*, 1662−1670.
(70) Lee, A. S. GRP78 Induction in Cancer: Therapeutic and Prognostic Implications: Figure 1. *Cancer Res.* **2007**, *67*, 3496−3499.
(71) Pillich, H.; Loose, M.; Zimmer, K.-P.; Chakraborty, T. Diverse roles of endoplasmic reticulum stress sensors in bacterial infection. *Mol. Cell. Pediatr.* **2016**, *3*, 1−6.
(72) Abuaita, B. H.; Burkholder, K. M.; Boles, B. R.; O'Riordan, M. X. The Endoplasmic Reticulum Stress Sensor Inositol-Requiring Enzyme 1α Augments Bacterial Killing through Sustained Oxidant Production. *mBio* **2015**, *6*, e00705−e00715.
(73) Li, J.; Sasaki, H.; Sheng, Y. L.; Schneiderman, D.; Xiao, C. W.; Kotsuji, F.; Tsang, B. K. Apoptosis and chemoresistance in human ovarian cancer: is Xiap a determinant? *Biol. Signals Recept.* **2000**, *9*, 122−130.
(74) Alvero, A. B.; Chen, W.; Sartorelli, A. C.; Schwartz, P.; Rutherford, T.; Mor, G. Triapine (3-aninopyridine-2-carboxaldehyde thiosemicarbazone) Induces Apoptosis in Ovarian Cancer Cells. *J. Soc. Gynecol. Invest.* **2016**, *13*, 145−152.
(75) Karlsson, H.; Fryknäs, M.; Strese, S.; Gullbo, J.; Larsson, R.; Sjöblom, T.; Pandzic, T.; Nygren, P.; Westman, G.; Bremberg, U. Mechanistic characterization of a copper containing thiosemicarbazone with potent antitumor activity. *Oncotarget* **2017**, *8*, 30217−30234.
(76) Bisceglie, F.; Alinovi, R.; Pinelli, S.; Galetti, M.; Pioli, M.; Tarasconi, P.; Mutti, A.; Goldoni, M.; Pelosi, G. Autophagy and apoptosis: studies on the effects of bisthiosemicarbazone copper(II) complexes on p53 and p53-null tumour cell lines. *Metallomics* **2016**, *8*, 1255−1265.
(77) Hancock, C. N.; Stockwin, L. H.; Han, B.; Divelbiss, R. D.; Jun, J. H.; Malhotra, S. V.; Hollingshead, M. G.; Newton, D. L. A copper chelate of thiosemicarbazone NSC 689534 induces oxidative/ER stress and inhibits tumor growth in vitro and in vivo. *Free Radical Biol. Med.* **2011**, *50*, 110−121.
(78) De Bortoli, M.; Taverna, E.; Bongarzone, I.; Maffioli, E.; Tedeschi, G.; Casalini, P.; Crisafi, F.; Kumar, V.; Polli, D.; Caccia, C. Lipid accumulation in human breast cancer cells injured by iron depletors. *J. Exp. Clin. Cancer Res.* **2018**, *37*, 75.
(79) Gans, P.; Sabatini, A.; Vacca, A. Investigation of equilibria in solution. Determination of equilibrium constants with the HYPERQUAD suite of programs. *Talanta* **1996**, *43*, 1739−1753.
(80) Zékány, L.; Nagypál, I. In *Computational Methods for the Determination of Stability Constants*; Leggett, D. L., Ed.; Plenum Press: New York, 1985; p 291.
(81) Rockenbauer, A.; Szabó-Plánka, T.; Árkosi, Z.; Korecz, L. A two-dimensional (magnetic field and concentration) electron paramagnetic resonance method for analysis of multispecies complex equilibrium systems. Information content of EPR spectra. *J. Am. Chem. Soc.* **2001**, *123*, 7646−7654.
(82) Enyedy, É. A.; Hollender, D.; Kiss, T. Lipophilicity of kinetically labile metal complexes through the example of antidiabetic Zn(II) and VO(IV) compounds. *J. Pharm. Biomed. Anal.* **2011**, *54*, 1073−1081.
(83) *SAINT-Plus*, version 8.32B and APEX2; Bruker-Nonius AXS Inc.: Madison, WI, 2016.
(84) *CrysAlis RED*, Version 1.171.36.32; Oxford Diffraction Ltd., 2003.
(85) Sheldrick, G. M. A short history of SHELX. *Acta Crystallogr.* **2008**, *A64*, 112−122.
(86) Burnett, M. N.; Johnson, G. K. *ORTEPIII*. Report ORNL-6895; OAK Ridge National Laboratory: Tennessee, 1996.
(87) Mooij, W. T. M.; Verdonk, M. L. General and targeted statistical potentials for protein-ligand interactions. *Proteins* **2005**, *61*, 272−287.
(88) Eldridge, M. D.; Murray, C. W.; Auton, T. R.; Paolini, G. V.; Mee, R. P. Empirical scoring functions: I. The development of a fast empirical scoring function to estimate the binding affinity of ligands in receptor complexes. *J. Comput.-Aided Mol. Des.* **1997**, *11*, 425−445.
(89) Verdonk, M. L.; Cole, J. C.; Hartshorn, M. J.; Murray, C. W.; Taylor, R. D. Improved protein-ligand docking using GOLD. *Proteins* **2003**, *52*, 609−623.
(90) Korb, O.; Stützle, T.; Exner, T. E. Empirical Scoring Functions for Advanced Protein−Ligand Docking with PLANTS. *J. Chem. Inf. Model.* **2009**, *49*, 84−96.
(91) *Schrödinger Small-Molecule Drug Discovery Suite 2015-4*: QikProp, 4.6; 2015.
(92) ChemAxon-Marvin, *ChemAxon. Ltd: 15.7.13.0*, 2015. http://www.chemaxon.com.
(93) Ioakimidis, L.; Thoukydidis, L.; Mirza, A.; Naeem, S.; Reynisson, J. Benchmarking the reliability of QikProp. Correlation between experimental and predicted values. *QSAR Comb. Sci.* **2008**, *27*, 445.
(94) Clinical and Laboratory Standards Institute. *Methods for Dilution Antimicrobial Susceptibility Test for Bacteria that Grow Aerobically*; Approved Standard, CLSI Document M7-A7, 7th ed.; Clinical and Laboratory Standards Institute: Wayne, PA 2006.

DOI: 10.1021/acs.jmedchem.8b01031
J. Med. Chem. 2019, 62, 512−530